

Haverford College

Haverford Scholarship

Faculty Publications

Physics

2006

The Parkes Multibeam Pulsar Survey: VI. Discovery and Timing of 142 Pulsars and a Galactic Population Analysis

Duncan R. Lorimer

A. J. Faulkner

A. G. Lyne

Richard N. Manchester

Fronefield Crawford

Haverford College, fcrawford@haverford.edu

Follow this and additional works at: https://scholarship.haverford.edu/physics_facpubs

Repository Citation

"The Parkes Multibeam Pulsar Survey: VI. Discovery and Timing of 142 Pulsars and a Galactic Population Analysis" D. R. Lorimer, A. J. Faulkner, A. G. Lyne, R. N. Manchester, M. Kramer, M. A. McLaughlin, G. Hobbs, A. Possenti, I. H. Stairs, F. Camilo, M. Burgay, N. D'Amico, A. Corongiu, & F. Crawford, *Monthly Notices of the Royal Astronomical Society*, 372, 777 (2006).

This Journal Article is brought to you for free and open access by the Physics at Haverford Scholarship. It has been accepted for inclusion in Faculty Publications by an authorized administrator of Haverford Scholarship. For more information, please contact nmedeiro@haverford.edu.

The Parkes Multibeam Pulsar Survey – VI. Discovery and timing of 142 pulsars and a Galactic population analysis

D. R. Lorimer,^{1,2*} A. J. Faulkner,¹ A. G. Lyne,¹ R. N. Manchester,³ M. Kramer,¹
M. A. McLaughlin,^{1,2} G. Hobbs,³ A. Possenti,⁴ I. H. Stairs,⁵ F. Camilo,⁶ M. Burgay,⁴
N. D’Amico,^{4,7} A. Corongiu⁴ and F. Crawford⁸

¹University of Manchester, Jodrell Bank Observatory, Macclesfield, Cheshire SK11 9DL

²Department of Physics, West Virginia University, PO Box 6315, Morgantown, WV 26506, USA

³Australia Telescope National Facility, CSIRO, PO Box 76, Epping, NSW 1710, Australia

⁴INAF - Osservatorio Astronomico di Cagliari, Loc. Poggio dei Pini, Strada 54, 09012 Capoterra (CA), Italy

⁵Department of Physics & Astronomy, University of British Columbia, 6224 Agricultural Road, Vancouver, B.C. V6T 1Z1, Canada

⁶Columbia Astrophysics Laboratory, Columbia University, 550 West 120th Street, New York, NY 10027, USA

⁷Universita’ degli Studi di Cagliari, Dipartimento di Fisica, SP Monserrato-Sestu km 0,7, 90042 Monserrato (CA), Italy

⁸Department of Physics and Astronomy, Franklin & Marshall College, PO Box 3003, Lancaster, PA 17604, USA

Accepted 2006 July 28. Received 2006 July 28; in original form 2006 July 11

ABSTRACT

We present the discovery and follow-up observations of 142 pulsars found in the Parkes 20-cm multibeam pulsar survey of the Galactic plane. These new discoveries bring the total number of pulsars found by the survey to 742. In addition to tabulating spin and astrometric parameters, along with pulse width and flux density information, we present orbital characteristics for 13 binary pulsars which form part of the new sample. Combining these results from another recent Parkes multibeam survey at high Galactic latitudes, we have a sample of 1008 normal pulsars which we use to carry out a determination of their Galactic distribution and birth rate. We infer a total Galactic population of $30\,000 \pm 1100$ potentially detectable pulsars (i.e. those beaming towards us) having 1.4-GHz luminosities above 0.1 mJy kpc^2 . Adopting the Tauris & Manchester beaming model, this translates to a total of $155\,000 \pm 6000$ active radio pulsars in the Galaxy above this luminosity limit. Using a pulsar current analysis, we derive the birth rate of this population to be 1.4 ± 0.2 pulsars per century. An important conclusion from our work is that the inferred radial density function of pulsars depends strongly on the assumed distribution of free electrons in the Galaxy. As a result, any analyses using the most recent electron model of Cordes & Lazio predict a dearth of pulsars in the inner Galaxy. We show that this model can also bias the inferred pulsar scaleheight with respect to the Galactic plane. Combining our results with other Parkes multibeam surveys we find that the population is best described by an exponential distribution with a scaleheight of 330 pc. Surveys underway at Parkes and Arecibo are expected to improve the knowledge of the radial distribution outside the solar circle, and to discover several hundred new pulsars in the inner Galaxy.

Key words: methods: statistical – stars: neutron – pulsars: general.

1 INTRODUCTION

The Parkes multibeam pulsar survey of the Galactic plane is the most successful large-scale search for pulsars so far undertaken. Five previous papers in this series have presented timing parameters for 600 newly discovered pulsars and have discussed various aspects of the survey results. A detailed description of the 13-beam

20-cm receiver system and data reduction software can be found in Manchester et al. (2001). Preliminary remarks about the population statistics were made by Morris et al. (2002). Kramer et al. (2003) discussed the association of young pulsars with unidentified EGRET sources and gave evidence for pulsars tracing the spiral-arm structure of the Galaxy. Hobbs et al. (2004) discussed the detection of previously known pulsars in the survey. Finally, Faulkner et al. (2004) implemented and discussed improved processing and candidate selection strategies for the entire survey data base with an emphasis on finding binary and millisecond pulsars.

*E-mail: Duncan.Lorimer@mail.wvu.edu

In this paper, we present the discovery parameters and provide timing solutions for a further 142 new pulsars. This brings the total number of pulsars found in the survey to 742. Although future searches of the data may produce a few additional discoveries, the vast majority of ‘normal’ (i.e. non-recycled) pulsars detectable by the survey have now been found. It is therefore appropriate to use this sample to place new constraints on the Galactic distribution and birth rate of normal pulsars. Of particular interest is the distribution in Galactocentric radius. Due to severe selection effects on low-frequency (<1 GHz) pulsar surveys, earlier studies (see e.g. Taylor & Manchester 1977) were somewhat hampered by small number statistics in the inner Galaxy and were often limited to local population analyses (see e.g. Lyne et al. 1998). In recent years, with the discovery of a larger number of pulsars in 1.4-GHz surveys there has been a growing body of evidence which suggests a deficit of pulsars in the inner Galaxy relative to a simple model where the radial density profile follows a Gaussian distribution (Johnston 1994; Lorimer 2004; Yusifov & Küçük 2004). One of the main goals of this paper is to use the new sample, which provides greatly improved pulsar statistics in the inner Galaxy, to provide an updated analysis on the Galactic distribution.

The plan for this paper is as follows. In Section 2 we present the basic timing parameters, pulse widths, mean profiles and flux densities for the 142 new pulsars. The sample contains a number of interesting individual objects, including several binary and millisecond pulsars which are discussed in Section 3. In Section 4, we describe our Galactic population analysis. The main conclusions from this work are summarized in Section 5.

2 DISCOVERY AND TIMING OF 142 PULSARS

The pulsars presented here were discovered primarily using the processing schemes described by Faulkner et al. (2004). In brief, to compensate for the dispersive effects of the interstellar medium, data from each telescope beam were de-dispersed at 325 different trial values of dispersion measure (DM) spanning the range 0–2203 cm⁻³ pc. The de-dispersed time-series were then subjected in turn to: a standard fast Fourier transform (FFT) analysis to search for periodic signals (Manchester et al. 2001), a segmented FFT search for accelerated signals from binary pulsars (Faulkner et al. 2004), a fast-folding algorithm (Kramer et al., in preparation) primarily sensitive to periods in the range 1–10 s and a search for dispersed single pulses (McLaughlin et al. 2006). Pulsar candidates from all but the latter search were selected using a graphical tool which displayed various aspects of the search parameter space, e.g. signal-to-noise ratio (S/N) versus pulse period. Promising candidates were noted for later re-observation at Parkes.

Following the confirmation and positional refinement procedures described by Morris et al. (2002), each pulsar was observed regularly for at least one year using one or more of the Parkes, Lovell and Arecibo telescopes. The observing systems used at Parkes and at Jodrell Bank are described by Manchester et al. (2001) and Morris et al. (2002) respectively. The Arecibo timing is described by Hobbs et al. (2004) and Stairs et al. (2005). For each pulsar, pulse times of arrival (TOAs) were determined from the individual observations using standard pulsar timing techniques (see e.g. Lorimer & Kramer 2005) implemented in the PSRCHIVE software package (Hotan, van Straten & Manchester 2004).¹ A model containing the spin, as-

tronomical and (if necessary) any binary parameters was fitted to the TOAs using the TEMPO timing package.²

The positional information from these fits is provided in equatorial and Galactic coordinates in Table 1. Subsequent columns in this table contain information on the discovery of each pulsar: the beam number (corresponding to the 13 beams of the multibeam receiver) for the strongest discovery observation, the radial distance between the centre of this beam and the position of the pulsar (distances greater than one beam radius can occur if the pulsar scintillates or nulls or the closest pointing was contaminated by interference) and the S/N of the profile³ during this observation. The observations used to form TOAs were added together to provide a characteristic pulse profile for each pulsar at 1400 MHz (Fig. 1). The final three columns in Table 1 contain the flux densities measured from these mean profiles (for further details, see Manchester et al. 2001), pulse widths at 50 and 10 per cent of the pulse height. The 10 per cent width is not measurable for pulsars with mean profiles that have poor S/N. For profiles containing multiple components the widths are measured across the entire profile.

The rotational parameters from the timing analyses are given in Table 2. In column order, this table provides each pulsar’s name, Solar system barycentric pulse period, period derivative, epoch of pulse period, the number of TOAs used in the timing solution, the MJD range covered by the timing observations, rms value of the observed – model residuals and the DM. The data have been folded in turn at two and three times the tabulated periods to confirm that they represent the fundamental periods of the pulsars, rather than a harmonic.

Various derived parameters for the new pulsars are presented in Table 3. For each pulsar, we list the base-10 logarithms of the characteristic age, surface dipole magnetic field strength and rate of loss of rotational energy. The final columns contain the pulsar distances, height above the Galactic plane and luminosities.⁴ The distances are computed from their DMs assuming the Taylor & Cordes (1993) and Cordes & Lazio (2002) models for the Galactic distribution of free electrons. The former is used for consistency with earlier papers in this series. The latter is more up-to-date and used for the population analysis in Section 4.2.

3 DISCUSSION OF INDIVIDUAL OBJECTS

The 7.7-s pulsar J1001–5939 has the longest spin period in our sample, and is the second longest known for a radio pulsar after the 8.5-s pulsar J2144–3933 (Young, Manchester & Johnston 1999). Unlike PSR J2144–3933, the much larger period derivative measured for J1001–5939 means that the pulsar lies above the ‘death line’ in the $P - \dot{P}$ diagram (Ruderman & Sutherland 1975). However, its implied dipole surface magnetic field is below the quantum critical limit (Baring & Harding 2001). As a result, PSR J1001–5939 does not pose any serious problems to theories of radio emission. Although the initial survey detection of this pulsar was registered in its second harmonic in the standard FFT search, its detection was much more significant using the fast-folding algorithm. Full details

²<http://www.atnf.csiro.au/research/pulsar/tempo>

³Throughout this paper we discuss S/N measurements made in the time domain, i.e. determined directly from the integrated pulse profile (for further details, see Lorimer & Kramer 2005).

⁴Note that throughout this paper we will use the term luminosity L to describe the quantity $L = Sd^2$, where S is the flux density and d is the distance. As this omits any geometrical and beaming factors, this quantity is often referred to as a pseudoluminosity (see e.g. Arzoumanian, Chernoff & Cordes 2002).

¹<http://psrchive.sourceforge.net>

Table 1. Positions, flux densities and pulse widths for 142 pulsars discovered in this phase of the Parkes multibeam pulsar survey. Radial angular distances are given in units of beam radii. Pulse widths at 10 per cent of the peak are given only for high S/N profiles.

PSR J	RA (J2000) (h m s)	Dec. (J2000) (° ′ ″)	l (°)	b (°)	Beam	Radial distance	S/N	S_{1400} (mJy)	W_{50} (ms)	W_{10} (ms)
0733–2345	07:33:24.60(4)	–23:45:56.2(11)	238.71	–2.03	4	0.50	9.0	0.07	19	63
0932–5327	09:32:22.86(14)	–53:27:11.0(16)	275.89	–1.38	8	0.35	25.1	0.15	59	93
1001–5939	10:01:32.23(14)	–59:39:17.8(7)	282.94	–3.55	7	0.81	111.2	0.15	39	160
1020–6026	10:20:11.40(7)	–60:26:06.8(5)	285.30	–2.85	12	0.52	12.6	0.14	14	26
1107–5907	11:07:34.46(4)	–59:07:18.7(3)	289.94	1.11	4	0.90	14.8	0.18	9.3	170
1125–6014	11:25:55.2180(4)	–60:14:06.608(4)	292.50	0.89	12	0.80	9.3	0.05	0.21	1.8
1148–5725	11:48:28.53(19)	–57:25:12.6(17)	294.51	4.42	3	0.82	18.2	0.12	51	68
1216–6410	12:16:07.3396(9)	–64:10:09.226(8)	299.10	–1.56	2	0.50	15.7	0.05	0.22	3
1308–5844	13:08:21.08(3)	–58:44:13.8(4)	305.13	4.06	6	0.38	54.7	0.21	5.9	15
1355–5747	13:55:36.95(15)	–57:47:15(3)	311.43	4.02	6	0.42	46.2	0.36	29	57
1357–6429	13:57:02.43(2)	–64:29:30.2(1)	309.92	–2.51	2	0.96	34.2	0.44	15	31
1405–5641	14:05:12.41(4)	–56:41:24.2(7)	312.97	4.74	3	0.64	15.1	0.10	12	29
1439–5501	14:39:39.7420(4)	–55:01:23.621(6)	318.10	4.63	9	0.34	17.3	0.42	1.7	3.4
1519–5734	15:19:47.59(6)	–57:34:13.6(7)	321.80	–0.24	9	0.74	24.0	0.45	40	82
1519–6106	15:19:35.81(11)	–61:06:54.6(12)	319.88	–3.22	4	0.01	38.3	0.19	25	47
1538–5732	15:38:18.18(3)	–57:32:29.3(4)	323.87	–1.62	1	0.28	20.1	0.35	5	13
1558–5756	15:58:30.53(3)	–57:56:26.1(4)	325.73	–3.60	1	0.38	63.1	0.19	9.5	19
1600–5916	16:00:35.0(4)	–59:16:59(3)	325.06	–4.80	5	0.54	24.9	0.33	127	146
1604–4718	16:04:29.41(4)	–47:18:47.9(6)	333.40	3.81	4	0.87	18.5	0.22	11	23
1611–5847	16:11:51.313(6)	–58:47:42.33(9)	326.46	–5.41	6	0.75	53.1	0.11	2.8	6.5
1617–4608	16:17:35.105(13)	–46:08:36.5(3)	335.84	3.14	1	0.92	20.7	0.15	7.7	17
1622–4347	16:22:30.060(18)	–43:47:21.4(3)	338.12	4.20	13	0.57	19.1	0.18	9.8	17
1624–4411	16:24:21.361(18)	–44:11:33.8(5)	338.07	3.68	10	0.56	39.5	0.48	8.1	50
1624–4613	16:24:18.7(3)	–46:13:02(9)	336.62	2.26	10	0.56	–	0.39	168	197
1627–4706	16:27:28.75(4)	–47:06:50.2(7)	336.35	1.25	1	0.76	9.1	0.10	9	23
1631–4155	16:31:18.33(7)	–41:55:03.7(20)	340.60	4.33	9	0.78	23.6	0.19	14	28
1634–5107	16:34:04.91(11)	–51:07:44.8(15)	334.17	–2.29	7	0.77	38.7	0.35	14	39
1637–4450	16:37:53.15(3)	–44:50:26.3(8)	339.25	1.48	12	1.15	15.4	0.40	14	107
1638–3815	16:38:37.349(18)	–38:15:03.4(7)	344.26	5.76	3	0.99	28.0	0.62	57	74
1638–4725	16:38:12.94(11)	–47:25:32(3)	337.36	–0.30	5	1.41	14.9	0.32	52	132
1643–4505	16:43:36.97(9)	–45:05:46.0(16)	339.73	0.55	1	0.92	17.3	0.28	9	19
1646–5123	16:46:36.35(4)	–51:23:14.6(5)	335.28	–3.93	3	0.81	20.9	0.17	15	24
1649–3805	16:49:48.222(19)	–38:05:59.1(3)	345.82	4.19	13	0.56	61.9	1.0	8	34
1650–4921	16:50:35.100(6)	–49:21:03.88(12)	337.25	–3.11	9	1.51	15.9	0.16	3.8	–
1653–4030	16:53:34.23(14)	–40:30:01.4(48)	344.42	2.11	12	0.88	16.2	0.40	122	161
1654–3710	16:54:44.426(19)	–37:10:57.1(9)	347.15	4.02	13	0.14	31.3	0.22	18	35
1656–3621	16:56:32.955(15)	–36:21:59.7(6)	348.01	4.25	6	0.22	42.9	0.29	20	40
1700–3611	17:00:49.32(5)	–36:11:53(3)	348.68	3.67	12	0.82	46.9	0.51	22	60
1700–4012	17:00:38.55(4)	–40:12:38.6(12)	345.49	1.23	11	0.59	10.2	0.13	16	27
1711–4322	17:11:10.561(12)	–43:22:53.1(5)	344.14	–2.24	12	0.79	11.1	0.26	7	16
1715–3859	17:15:37.89(3)	–38:59:25.1(9)	348.19	–0.35	12	0.80	15.0	0.54	61	128
1717–3953	17:17:25.55(20)	–39:53:55(8)	347.65	–1.16	3	0.42	26.5	0.78	299	367
1718–4539	17:18:11.90(4)	–45:39:15.9(9)	343.02	–4.58	4	0.86	12.9	0.08	11	36
1722–4400	17:22:46.517(12)	–44:00:33.2(3)	344.84	–4.32	12	0.77	17.3	0.22	4	8
1724–4500	17:24:25.8(3)	–45:00:15(4)	344.18	–5.12	1	0.83	12.3	0.05	28	38
1725–2852	17:25:09.9(3)	–28:52:22(17)	357.64	3.80	5	0.66	15.3	0.25	37	79
1728–4028	17:28:27.68(17)	–40:28:10(4)	348.38	–3.22	1	0.38	76.2	0.69	102	120
1730–2900	17:30:08.28(10)	–29:00:46(12)	358.12	2.82	11	0.21	21.4	0.13	23	44
1732–3426	17:32:07.18(7)	–34:26:05(3)	353.82	–0.51	8	0.51	13.5	0.24	14	33
1733–2533	17:33:25.86(8)	–25:33:11(18)	1.43	4.09	1	0.49	11.9	0.10	35	57

of this aspect of the survey data processing will appear elsewhere (Kramer et al., in preparation).

In addition to the new discoveries of rotating radio transient sources in the single-pulse search described by McLaughlin et al. (2006), one further pulsar, PSR J1624–4613, was only detectable in this part of the analysis. Our follow-up observations show that this

pulsar is only detectable about 70 per cent of the time. This and the lack of detection by the periodicity analysis suggests that this pulsar spends a significant fraction of time in a null state. The discovery of such pulsars alongside the radio transients highlights the value of the single-pulse search analysis as an important component of pulsar survey pipelines.

Table 1 – *continued*

PSR J	RA (J2000) (h m s)	Dec. (J2000) (° ′ ″)	<i>l</i> (°)	<i>b</i> (°)	Beam	Radial distance	S/N	S_{1400} (mJy)	W_{50} (ms)	W_{10} (ms)
1733–2837	17:33:33.90(5)	–28:37:33(8)	358.86	2.40	10	0.24	14.2	0.07	12	20
1734–2415	17:34:41.6(3)	–24:15:20(90)	2.68	4.55	13	0.49	23.9	0.29	31	51
1736–2457	17:36:45.44(8)	–24:57:50(22)	2.33	3.78	9	0.79	64.0	0.52	62	103
1738–2330	17:38:08.8(3)	–23:30:47(103)	3.73	4.28	11	0.68	21.0	0.48	35	69
1739–3951	17:39:38.25(4)	–39:52:00.3(8)	350.04	–4.69	3	4.45	11.8	0.12	9	19
1741–2719	17:41:35.06(4)	–27:19:23(7)	0.91	1.60	7	0.39	23.7	0.20	14	30
1742–3957	17:42:04.43(19)	–39:57:22(9)	350.21	–5.13	7	1.03	18.0	0.14	65	120
1744–3922	17:44:02.675(10)	–39:22:21.1(4)	350.91	–5.15	4	1.26	26.5	0.20	3.4	7.3
1750–2043	17:50:18.4(5)	–20:43:08(75)	7.59	3.33	10	0.58	21.1	0.24	358	432
1751–2857	17:51:32.6965(2)	–28:57:46.50(3)	0.65	–1.12	11	0.91	18.5	0.06	0.25	0.74
1753–1914	17:53:35.171(12)	–19:14:58(3)	9.25	3.41	2	0.23	49.4	0.13	10	14
1754–3510	17:54:54.616(7)	–35:10:43.0(5)	355.64	–4.88	4	0.50	101.8	0.47	4.1	13
1755–1650	17:55:11.648(18)	–16:50:41(3)	11.53	4.29	4	0.52	17.0	0.13	14	26
1756–2251	17:56:46.6332(2)	–22:51:59.4(2)	6.50	0.95	7	0.87	19.6	0.6	0.78	1.6
1758–2846	17:58:15.41(3)	–28:46:02(5)	1.56	–2.29	7	0.65	32.4	0.20	4.4	30
1759–1736	17:59:28.16(7)	–17:36:10(7)	11.38	3.03	9	0.26	11.2	0.12	18	44
1801–1417	18:01:51.0764(5)	–14:17:34.50(5)	14.55	4.16	12	1.28	37.7	0.17	0.6	1.3
1801–3458	18:01:52.66(11)	–34:58:37(7)	356.52	–6.02	12	0.65	12.7	0.11	47	110
1802–2124	18:02:05.3352(3)	–21:24:03.6(3)	8.38	0.61	4	0.93	15.2	0.77	0.37	0.74
1805–1504	18:05:06.10(17)	–15:04:36(18)	14.25	3.09	7	1.10	94.8	2.2	229	340
1808–1020	18:08:45.634(6)	–10:20:48.3(4)	18.83	4.60	9	0.89	34.9	0.23	8	23
1808–1726	18:08:42.3(3)	–17:26:27(42)	12.60	1.19	5	0.28	18.9	0.39	66	–
1808–2701	18:08:13.23(4)	–27:01:21(9)	4.16	–3.36	11	0.88	16.5	0.15	23	80
1811–2439	18:11:55.53(3)	–24:39:53(9)	6.63	–2.95	1	0.66	37.3	0.26	15	24
1812–2526	18:12:32.30(3)	–25:26:38(7)	6.01	–3.45	11	0.80	13.1	0.18	12	19
1814–0618	18:14:41.26(7)	–06:18:01.7(33)	23.10	5.23	8	0.45	16.9	0.58	48	194
1816–0755	18:16:24.543(6)	–07:55:22.5(4)	21.87	4.09	8	0.85	23.7	0.17	6	17
1817–0743	18:17:49.79(5)	–07:43:18.9(14)	22.21	3.88	9	0.32	13.6	0.25	13	34
1819–1318	18:19:43.66(5)	–13:18:42(5)	17.50	0.83	13	0.46	13.7	0.16	23	41
1820–0509	18:20:22.728(7)	–05:09:38.5(4)	24.78	4.52	5	0.63	32.4	0.25	9	18
1821–0256	18:21:10.310(20)	–02:56:38.6(10)	26.84	5.37	1	0.98	9.7	0.19	10	25
1822–0848	18:22:51.86(8)	–08:48:59.0(11)	21.83	2.26	1	0.35	28.7	0.04	18	55
1824–0127	18:24:53.43(4)	–01:27:51.4(18)	28.59	5.23	4	1.18	31.7	0.59	20	81
1824–2233	18:24:10.32(5)	–22:33:11(16)	9.82	–4.44	7	0.34	49.6	0.22	13	32
1824–2328	18:24:28.64(19)	–23:28:17(61)	9.04	–4.92	2	1.12	61.0	0.32	35	51
1827–0750	18:27:02.735(6)	–07:50:19.2(6)	23.18	1.80	1	0.38	119.1	1.4	10	36
1828–2119	18:28:21.56(5)	–21:19:56(11)	11.36	–4.73	4	0.75	37.5	0.38	22	34
1829+0000	18:29:47.14(3)	+00:00:08.5(11)	30.46	4.82	6	1.07	20.4	0.43	16	30
1830–0052	18:30:30.70(5)	–00:52:54.0(15)	29.76	4.25	4	0.23	10.5	0.04	9	16
1830–0131	18:30:19.612(12)	–01:31:48.1(6)	29.16	3.99	7	1.43	13.1	0.35	11	18
1830–1414	18:30:00.35(4)	–14:14:37(4)	17.84	–1.81	2	0.18	11.6	0.10	10	22
1831–0952	18:31:34.304(16)	–09:52:01.7(11)	21.90	–0.13	11	0.59	13.9	0.33	8	14
1832+0029	18:32:50.7(3)	+00:29:27(18)	31.25	4.36	10	0.87	12.5	0.14	7	15
1834–0031	18:34:51.093(14)	–00:31:34.3(6)	30.57	3.45	4	1.04	14.3	0.17	5	13
1834–1855	18:34:45.94(5)	–18:55:59(6)	14.19	–4.98	5	1.00	27.2	0.48	32	71
1835–0349	18:35:12.946(12)	–03:49:09.9(9)	27.68	1.86	7	0.57	26.6	0.16	15	28
1835–0944	18:35:46.66(9)	–09:44:29(3)	22.49	–0.99	1	0.30	18.8	0.41	7	19
1835–0946	18:35:44.86(9)	–09:46:38(3)	22.45	–1.00	1	0.56	21.2	0.18	4	7.2
1835–1548	18:35:50.33(10)	–15:48:38(10)	17.09	–3.78	6	0.51	9.7	0.06	17	42
1836–1324	18:36:52.287(9)	–13:24:33.6(5)	19.35	–2.91	4	3.83	20.0	0.10	2.4	41

The youngest pulsar in our sample, PSR J1357–6429, has been extensively discussed by Camilo et al. (2004). This pulsar, which has suffered a Vela-like glitch, is possibly associated with the radio supernova remnant G309.8–2.6. We have searched for coincidences between the newly discovered pulsars that lie within the bounds of the 231 supernova remnants in Green’s cat-

alogue as well as the 35 remnants recently found in the inner Galaxy (Brogan et al. 2006). Although five additional matches were found (G4.2–3.5 and J1808–2701; G27.8+0.6 and J1839–0436; G321.9–0.3 and J1519–5734; G343.0–6.0 and J1718–4539; and G343.0–6.0 J1724–4500) none of the pulsars have characteristic ages below 6×10^5 yr or an angular offset less than 0.45

Table 1 – continued

PSR J	RA (J2000) (h m s)	Dec. (J2000) (° ′ ″)	l (°)	b (°)	Beam	Radial distance	S/N	S_{1400} (mJy)	W_{50} (ms)	W_{10} (ms)
1837+0053	18:37:28.45(7)	+00:53:13(3)	32.13	3.51	7	1.17	18.7	0.34	49	108
1839–0436	18:39:00.064(9)	–04:36:57.5(7)	27.41	0.65	8	0.65	10.9	0.23	6	12
1839–1238	18:39:43.708(19)	–12:38:40.7(18)	20.35	–3.18	4	3.73	75.7	0.37	30	53
1840+0214	18:40:34.087(19)	+02:14:54.7(6)	33.70	3.44	3	0.31	13.8	0.07	10	22
1840–0840	18:40:51.9(4)	–08:40:29(15)	24.01	–1.62	2	0.03	61.7	1.00	188	343
1840–1207	18:40:53.782(8)	–12:07:32.6(6)	20.94	–3.20	8	0.77	24.2	0.22	15	22
1841+0130	18:41:17.761(8)	+01:30:16.9(3)	33.12	2.94	12	1.06	11.4	0.06	6	11
1841–1404	18:41:34.3(4)	–14:04:19(41)	19.28	–4.23	7	0.15	19.0	0.18	17	122
1842+0257	18:42:30.93(4)	+02:57:58.8(14)	34.56	3.34	4	1.06	55.0	0.26	52	85
1842+0358	18:42:17.022(6)	+03:58:35.3(3)	35.43	3.85	6	0.63	20.2	0.09	4	8
1842+0638	18:42:10.002(17)	+06:38:15.0(7)	37.80	5.07	10	0.98	16.1	0.21	13	20
1843–1507	18:43:33.607(7)	–15:07:03.0(8)	18.56	–5.13	9	0.63	46.1	0.17	7	18
1845+0623	18:45:08.59(3)	+06:23:57.6(9)	37.92	4.31	1	0.53	39.0	0.33	13	–
1845–0826	18:45:05.693(19)	–08:26:39.7(12)	24.69	–2.44	10	0.57	15.4	0.33	13	31
1845–1114	18:45:45.778(6)	–11:14:11.0(5)	22.28	–3.86	2	0.27	41.9	0.52	4	7
1845–1351	18:45:11.50(3)	–13:51:54.5(20)	19.86	–4.92	2	0.61	26.2	0.33	63	84
1846–0749	18:46:19.744(5)	–07:49:21.4(3)	25.39	–2.43	12	1.49	15.9	0.35	7	15
1848–0601	18:48:20.349(14)	–06:01:07.7(8)	27.22	–2.05	4	0.74	18.3	0.24	9	22
1848–1150	18:48:11.81(3)	–11:50:09.2(18)	22.01	–4.66	10	0.40	34.6	0.21	31	42
1849+0409	18:49:03.471(13)	+04:09:42.3(5)	36.37	2.42	4	0.23	33.1	0.10	9	17
1851–0114	18:51:16.41(3)	–01:14:13.4(13)	31.81	–0.53	2	0.87	18.5	0.28	22	44
1853+0853	18:53:22.07(11)	+08:53:17(3)	41.07	3.61	5	0.35	19.6	0.11	50	90
1853+1303	18:53:57.31 827(8)	+13:03:44.0884(17)	44.87	5.37	1	0.85	15.1	0.4	0.59	2.19
1856–0526	18:56:21.977(15)	–05:26:56.8(8)	28.64	–3.57	13	0.86	35.1	0.40	28	39
1901–0315	19:01:16.33(8)	–03:15:14.3(20)	31.15	–3.67	2	0.96	11.2	0.09	10	20
1901+0435	19:01:32.2(3)	+04:35:23(10)	38.17	–0.15	5	0.43	43.8	0.27	315	–
1901+0621	19:01:05.96(9)	+06:21:19(4)	39.69	0.76	10	0.76	14.2	0.47	43	–
1903–0258	19:03:30.343(11)	–02:58:15.6(7)	31.66	–4.04	9	0.37	22.3	0.14	7	–
1903+0925	19:03:55.18(20)	+09:25:55(6)	42.74	1.54	5	1.19	21.7	0.20	89	–
1904–0150	19:04:55.555(10)	–01:50:32.5(5)	32.83	–3.84	7	0.33	23.0	0.09	5	13
1906+0414	19:06:57.793(7)	+04:14:29.44(13)	38.48	–1.51	6	0.79	12.7	0.23	20	–
1907+1149	19:07:37.78(6)	+11:49:37.1(17)	45.29	1.83	11	0.55	25.3	0.13	15	30
1910–0112	19:10:15.7(4)	–01:12:06(14)	34.01	–4.74	10	0.66	11.0	0.07	50	89
1910+1256	19:10:09.70 041(6)	+12:56:25.5276(6)	46.56	1.80	12	0.16	17.2	0.5	0.14	0.43
1911+1347	19:11:55.2047(3)	+13:47:34.411(7)	47.52	1.81	1	0.31	36.3	0.08	0.15	0.44
1913+0904	19:13:21.061(8)	+09:04:45.4(4)	43.50	–0.68	4	0.54	33.3	0.07	3	6
1914+0219	19:14:23.794(8)	+02:19:47.8(3)	37.63	–4.04	13	0.62	172.0	0.75	16	24
1915+0227	19:15:02.122(5)	+02:27:47.77(16)	37.82	–4.12	9	0.69	56.3	0.55	7	27
1915+1410	19:15:35.416(12)	+14:10:51.5(3)	48.27	1.20	9	0.47	17.7	0.10	15	24
1921+0812	19:21:47.704(5)	+08:12:51.86(10)	43.71	–2.93	11	0.64	30.0	0.66	2	5
1927+0911	19:27:25.628(8)	+09:11:05.7(3)	45.22	–3.70	2	0.78	14.1	0.16	3	8
1941+1341	19:41:04.867(18)	+13:41:30.4(6)	50.80	–4.47	9	0.57	17.7	0.17	9	33

remnant radii. Such apparent coincidences are common and expected, given the high density of pulsars and supernova remnants along the Galactic plane (Gaensler & Johnston 1995; Lorimer, Lyne & Camilo 1998). To demonstrate this, we artificially shifted the remnant centres by 1° in Galactic longitude. The subsequent fake cross-correlation analysis resulted in six matches with similarly old pulsars and large angular offsets. We therefore do not believe any of the above coincidences are genuine pulsar–supernova remnant associations.

Several of the profiles shown in Fig. 1 exhibit the characteristic hallmark of interstellar scattering, i.e. an one-sided exponential tail. The most extreme example in the current sample is PSR J1901+0435, a 691-ms pulsar located at Galactic longitude

$l = 38^\circ$, which shows a scattering tail encompassing most of its rotational phase. Further study of this and other pulsars in the sample (see e.g. Bhat et al. 2004) will help improve models of the distribution of scattering material in the interstellar medium. These detections of highly scattered pulsars also suggest that, even at the survey frequency of 1.4 GHz, a number of nominally bright pulsars are not detectable due to scattering. Further surveys of the Galactic plane at even higher observing frequencies are required to detect these pulsars.

Our sample includes the two solitary millisecond pulsars J1801–1417 and J1911+1347, both originally announced by Faulkner et al. (2004). Improved timing parameters for these pulsars are given in Tables 1 and 2. These discoveries bring the sample

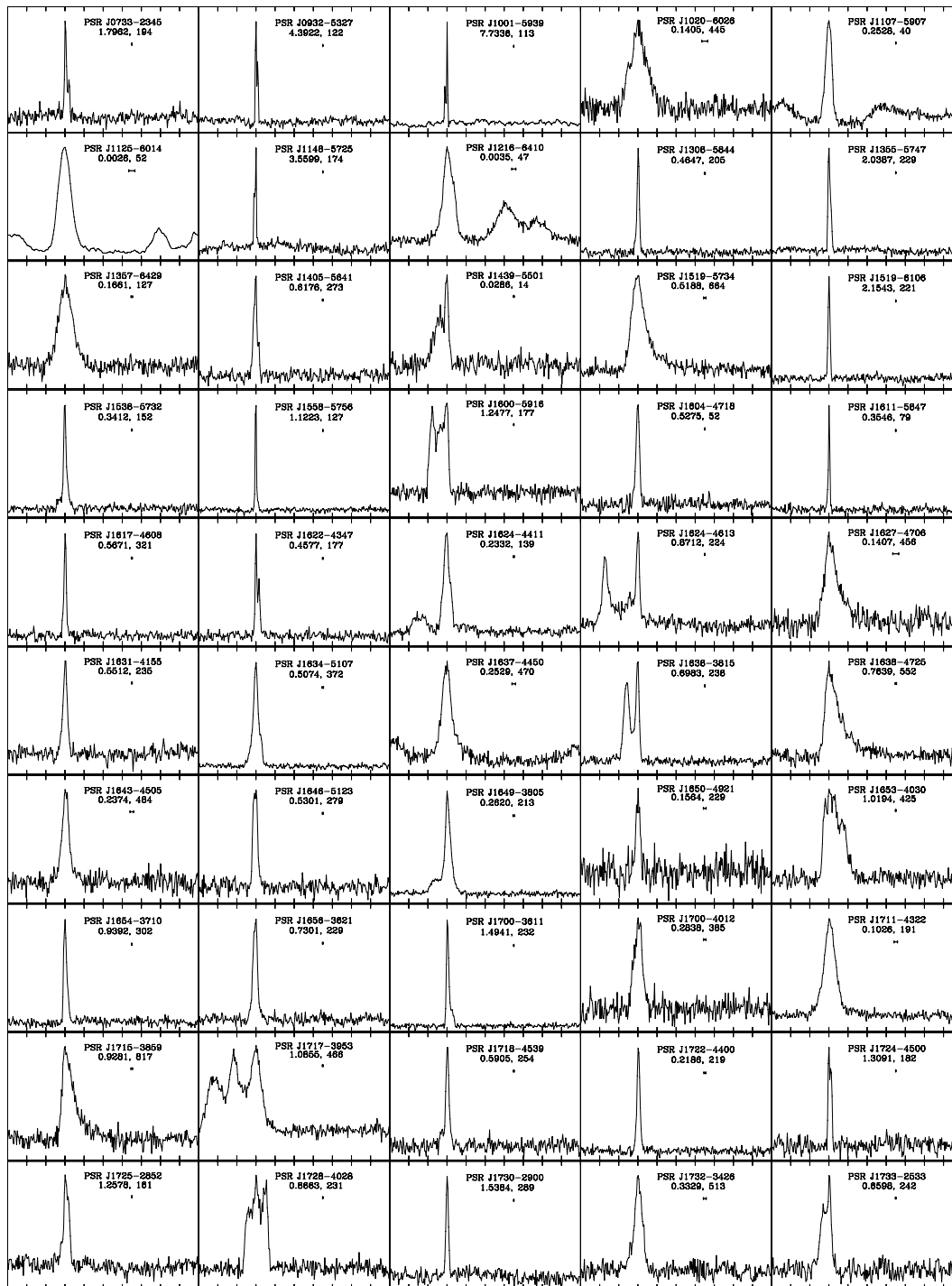


Figure 1. Mean 1400-MHz pulse profiles for 142 pulsars discovered in this phase of the multibeam survey. The highest point in the profile is placed at phase 0.3. Profiles have been compensated for the effects of the high-pass filter in the digitization system (Manchester et al. 2001). For each profile, the pulsar Jname, pulse period (s) and dispersion measure ($\text{cm}^{-3} \text{pc}$) are given. The small horizontal bar under the period indicates the effective resolution of the profile by adding the bin size to the effects of interstellar dispersion in quadrature.

of solitary millisecond pulsars known in the Galactic disc to 15. In keeping with the other isolated millisecond pulsars, these new sources have low radio luminosities compared to their counterparts with binary companions (Bailes et al. 1997; Kramer et al. 1998). As noted recently by Lommen et al. (2006) the difference in scale-heights of the binary and isolated pulsars, despite their having statistically identical velocity dispersions, also points to a difference

in luminosities for the two populations. It is currently unclear why the luminosity functions differ for the two populations.

Our sample includes 13 binary pulsars, the properties of which are summarized in Table 4. Of these, seven are discussed elsewhere: PSR J1638–4725 is a long-period binary pulsar in a highly eccentric orbit around a massive companion (Lyne et al., in preparation), PSR J1744–3922 is a short-period binary system with a low-mass

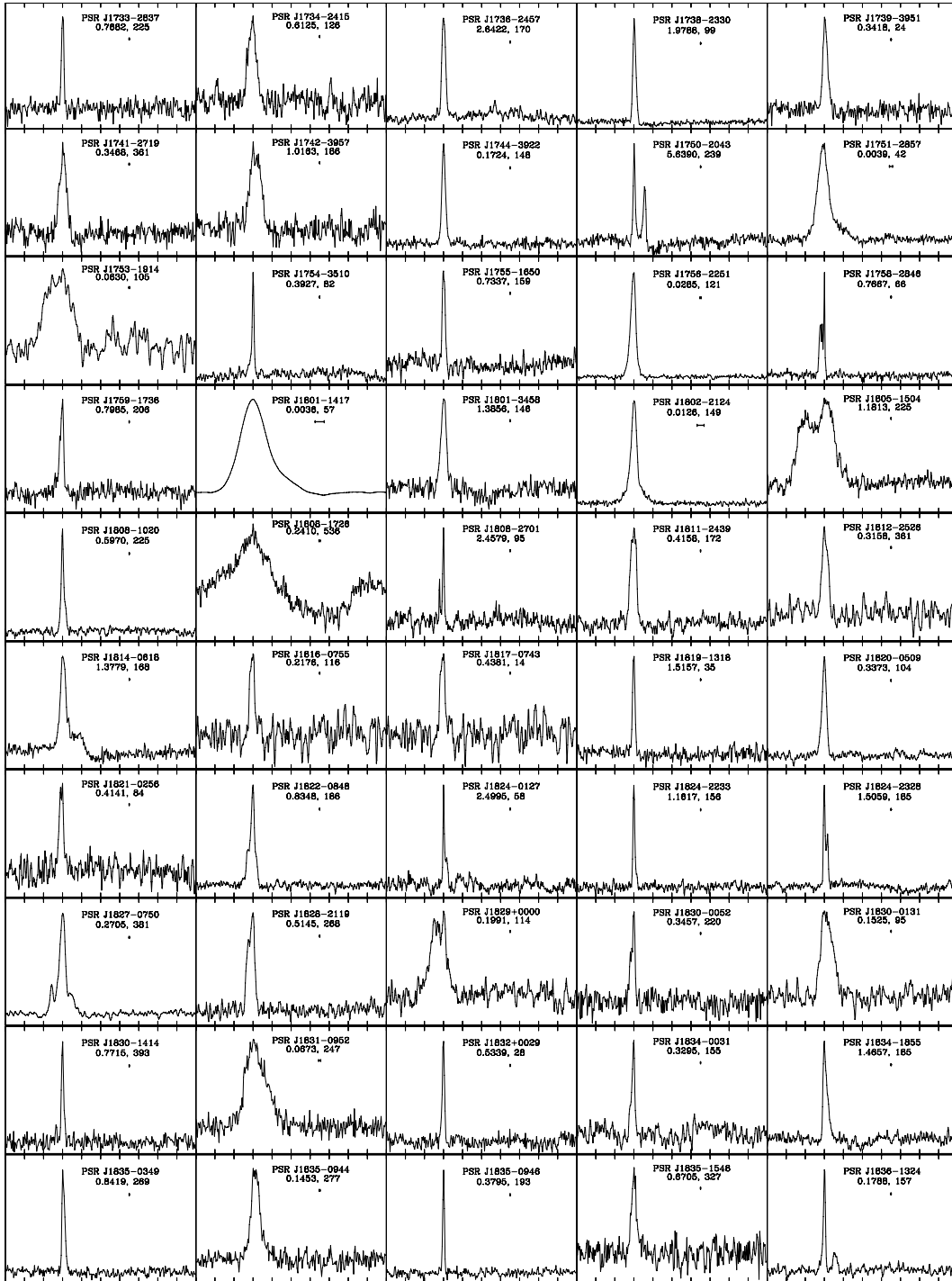


Figure 1 – continued

companion (Faulkner et al. 2004), PSR J1802–2124 has a companion of intermediate mass (Faulkner et al. 2004), PSR J1756–2251 is a double-neutron-star binary (Faulkner et al. 2005) and PSRs J1751–2857, J1853+1303 and J1910+1256 are millisecond pulsars in wide binary orbits (Stairs et al. 2005). In Tables 5 and 6, we provide orbital parameters for the remaining six binary systems.

PSRs J1711–4322 and J1822–0848 listed in Table 5 appear to be similar in character to PSR B0820+02; i.e. a long-period pulsar in a long-period orbit about a low-mass white dwarf companion.

PSRs J1125–6014, J1216–6410 and J1841+0130 are typical of other recycled pulsar binary systems with orbital periods of typically a few days and low-mass white dwarf companions. All of these binaries follow the spin period versus orbital period and magnetic field versus orbital period correlations discussed by van den Heuvel & Bitzaraki (1995) which support the largely empirical hypothesis that accretion on to the neutron star causes a reduction in the magnetic field strength (see e.g. Bhattacharya & van den Heuvel 1991).

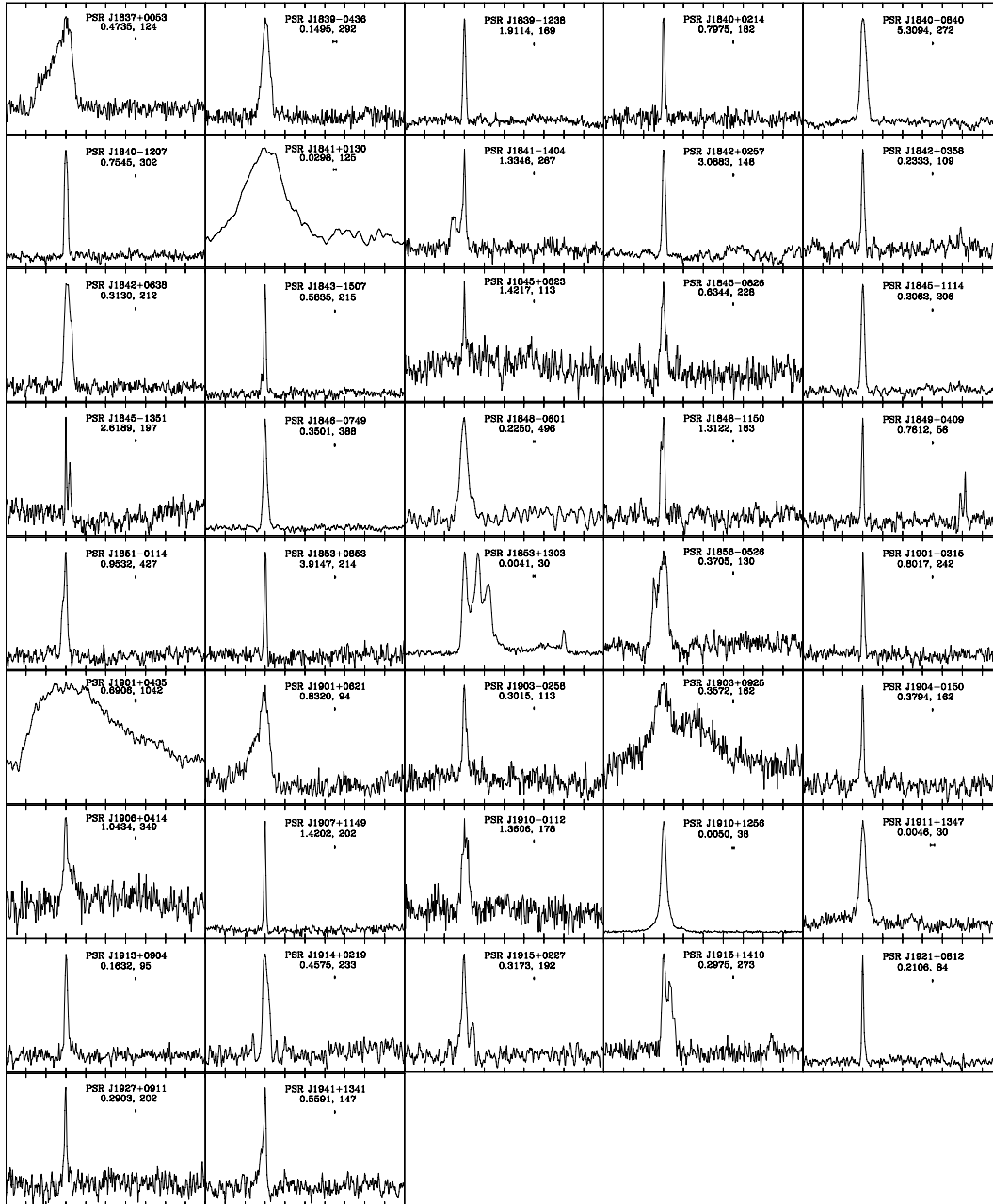


Figure 1 – continued

Another important tracer for the evolution of binary pulsars is the orbital period versus eccentricity correlation. According to the fluctuation–dissipation theory of Phinney (1992), a relationship between these parameters is expected for all pulsar–white dwarf binary systems which have undergone an extensive period of mass transfer. With the exception of PSRs J1841+0130 and J1853+1303, which deviate from the theoretical prediction by over an order of magnitude, the pulsar–white dwarf systems in our sample follow the $P_b - e$ correlation. As noted by Stairs et al. (2005), these two exceptions may simply be indicative of a natural scatter about the relationship. Further work is required to establish whether these deviations are indicative of a different evolutionary channel, such as the formation of the neutron star via accretion-induced collapse of a white dwarf in an accreting binary system (see e.g. Narayan & Popham 1989).

Slightly less typical is the 28-ms pulsar, PSR J1439–5501. This binary pulsar with a circular orbit of period 2 d has a minimum companion mass of $1.1 M_\odot$. It appears to be among the growing class of recycled pulsars with more massive CO white dwarf companions, the so-called ‘intermediate-mass binary pulsars’ (Camilo et al. 1996). Its closest known counterpart among the known systems is the 43-ms binary pulsar J1157–5112 (Edwards & Bailes 2001). Another likely intermediate-mass system is J1802–2124 for which the minimum companion mass is $0.8 M_\odot$ (Faulkner et al. 2004).

Related to the binary pulsars is the isolated pulsar PSR J1753–1914. With a spin period of 63 ms and a spin-down rate of only 2×10^{-18} , this pulsar appears to belong to the class of so-called ‘disrupted recycled pulsars’ (Lorimer et al. 2004). Since these objects have spin properties similar to the recycled pulsars in

Table 2. Periods, period derivatives and dispersion measures for 142 pulsars discovered in this phase of the Parkes multibeam pulsar survey. We also give the MJD of the epoch used for period determination, the number of TOAs included in the timing solution, the MJD range covered and the rms of the post-fit timing residuals.

PSR J	Period, P (s)	\dot{P} (10^{-15})	Epoch (MJD)	N_{TOA}	Data span (MJD)	Residual (ms)	DM (cm^{-3} pc)
0733–2345	1.79 624 970 117(10)	5.704(10)	530 14.0	27	525 74–534 54	1.8	194(3)
0932–5327	4.3921 587 127(6)	8.37(8)	530 99.0	21	527 72–534 26	4.0	122(11)
1001–5939	7.7336 402 649(8)	59.9(3)	530 69.0	39	528 26–533 12	2.0	113(3)
1020–6026	0.140 479 910 179(8)	6.7386(20)	531 28.0	31	528 54–534 03	1.4	445.0(20)
1107–5907	0.252 773 323 418(6)	0.009(10)	530 89.0	53	526 98–534 80	0.8	40.2(11)
1125–6014	0.0026 303 807 397 848(8)	0.00 000 401(9)	531 41.0	36	528 27–534 54	0.006	52.951(14)
1148–5725	3.5599 372 320(7)	11.1(13)	528 37.0	20	525 69–531 04	2.6	174(5)
1216–6410	0.003 539 375 658 423(3)	0.00 000 162(19)	533 91.0	40	530 51–537 32	0.011	47.40(3)
1308–5844	0.4646 997 488(7)	8.639(5)	515 60.0	24	526 92–531 04	0.4	205.6(11)
1355–5747	2.0386 738 254(4)	0.71(9)	535 13.0	31	532 83–537 42	3.3	229(3)
1357–6429	0.16 610 832 750(1)	360.184(1)	529 21.0	28	527 38–531 04	0.9	127.2(5)
1405–5641	0.61 757 468 514(4)	1.198(12)	528 98.0	21	526 92–531 04	0.6	273(3)
1439–5501	0.028 634 888 190 455(12)	0.0001 418(10)	532 00.0	170	529 15–537 16	0.025	14.56(5)
1519–5734	0.51 875 778 474(3)	4.273(5)	531 05.0	32	528 07–534 03	1.8	664(3)
1519–6106	2.15 430 706 064(14)	8.372(19)	530 48.0	36	526 95–534 02	1.8	221(3)
1538–5732	0.341 212 811 806(6)	4.5498(6)	518 03.0	40	513 00–523 06	1.0	152.7(8)
1558–5756	1.12 234 168 628(3)	186.406(4)	531 39.0	41	528 55–534 22	0.9	127.8(10)
1600–5916	1.2476 661 740(3)	0.89(7)	531 16.0	31	528 07–534 25	6.7	177(4)
1604–4718	0.527 465 874 211(20)	4.961(9)	528 97.0	20	526 95–531 00	0.5	52.0(16)
1611–5847	0.3545 503 166 464(18)	0.002(4)	530 71.0	33	527 39–534 03	0.2	79.9(13)
1617–4608	0.567 080 221 721(10)	16.4665(10)	531 29.0	34	528 55–534 03	0.6	321.5(12)
1622–4347	0.457 681 471 040(9)	5.051(4)	528 97.0	19	526 95–531 00	0.2	177(3)
1624–4411	0.233 164 076 390(4)	0.7992(8)	530 58.0	38	526 95–534 22	0.6	139.4(14)
1624–4613	0.8712 426 056(4)	<0.12	535 00.0	20	532 84–537 16	4.2	224.2(19)
1627–4706	0.140 745 806 053(6)	1.7305(6)	531 65.0	62	528 07–535 23	1.7	456.1(18)
1631–4155	0.55 124 125 377(4)	0.0088(73)	530 82.0	38	527 39–534 25	1.8	235(4)
1634–5107	0.50 735 578 252(6)	1.573(3)	528 60.0	49	522 94–534 26	3.4	372.8(20)
1637–4450	0.252 869 846 841(20)	0.5755(20)	532 83.0	28	530 78–534 89	0.4	470.7(8)
1638–3815	0.69 826 060 054(20)	0.077(3)	521 35.0	22	526 01–531 07	0.7	238.0(11)
1638–4725	0.7639 335(3)	4.8(9)	526 51.0	109	518 56–534 45	5.3	552.1(14)
1643–4505	0.237 383 081 875(17)	31.833(10)	529 23.0	17	527 39–531 07	0.9	484(3)
1646–5123	0.530 075 207 410(20)	2.099(12)	529 06.0	17	527 39–531 00	1.0	279(3)
1649–3805	0.262 025 692 969(7)	0.0367(14)	528 85.0	21	526 95–531 00	0.3	213.8(5)
1650–4921	0.1563 993 674 972(10)	1.81 873(20)	532 53.0	45	529 83–535 23	0.2	229.9(5)
1653–4030	1.01 937 155 664(16)	0.44(4)	531 39.0	36	528 55–534 22	5.8	425(8)
1654–3710	0.93 916 547 876(3)	0.735(3)	531 31.0	36	528 59–534 03	1.3	302.0(12)
1656–3621	0.730 133 707 454(16)	1.2752(16)	531 23.0	39	528 24–534 22	1.4	229(3)
1700–3611	1.49 409 061 528(16)	4.324(16)	528 28.0	27	525 84–531 00	1.2	232.7(12)
1700–4012	0.283 791 853 785(11)	0.099(4)	531 05.0	35	528 08–534 03	1.7	385(4)
1711–4322	0.1026 182 883 472(6)	0.02 666(5)	524 33.0	98	514 12–534 54	0.8	191.5(7)
1715–3859	0.92 810 750 775(3)	4.397(7)	530 97.0	35	527 72–534 22	6.4	817(5)
1717–3953	1.08 552 061 541(18)	0.033(19)	533 13.0	38	528 84–537 42	9.6	466(8)
1718–4539	0.59 047 278 772(3)	7.507(7)	531 05.0	29	528 08–534 03	1.0	254(6)
1722–4400	0.2185 540 958 272(15)	0.3738(4)	530 58.0	36	526 95–534 22	0.3	219.3(5)
1724–4500	1.3091 087 873(3)	3.51(12)	532 55.0	24	530 52–534 58	3.3	182(3)
1725–2852	1.257 787 625(10)	1.99(15)	521 97.0	20	526 92–531 03	3.7	161(10)
1728–4028	0.866 342 509(4)	0.23(6)	520 77.0	20	526 92–531 03	2.4	231(10)
1730–2900	1.5384 267 263(3)	8.85(8)	531 28.0	26	528 54–534 02	2.9	289(5)
1732–3426	0.33 288 667 881(4)	0.402(9)	523 59.0	23	521 46–525 72	1.2	513.5(18)
1733–2533	0.65 979 414 168(4)	2.1(5)	530 70.0	32	527 39–534 02	2.5	242(5)
1733–2837	0.76 818 455 674(6)	1.108(8)	531 28.0	22	528 54–534 02	1.7	225(5)

double-neutron-star binary systems, it was proposed by Camilo, Nice & Taylor (1993) that they are the result of the systems which disrupted at the time of the second supernova. As discussed by Lorimer et al. (2004), there appears to be a deficit of these sys-

tems among the known pulsar sample. Further investigations, especially using binary population syntheses, are required to investigate the frequency of these isolated recycled pulsars relative to double-neutron-star systems.

Table 2 – *continued*

PSR J	Period, P (s)	\dot{P} (10^{-15})	Epoch (MJD)	N_{TOA}	Data span (MJD)	Residual (ms)	DM (cm^{-3} pc)
1734–2415	0.61 252 373 999(12)	1.051(12)	531 64.0	56	528 56–534 71	6.4	126.3(7)
1736–2457	2.64 222 343 904(14)	3.43(3)	530 95.0	50	527 18–534 71	3.5	170(4)
1738–2330	1.97 884 743 163(4)	8.559(4)	532 06.0	33	526 95–537 16	1.0	99.3(18)
1739–3951	0.341 772 476 799(10)	0.02(5)	528 97.0	17	526 92–531 03	0.4	24.6(4)
1741–2719	0.346 796 929 142(19)	0.081(4)	528 36.0	23	525 69–531 03	1.2	361.9(4)
1742–3957	1.0163 491 951(4)	0.082(29)	531 24.0	29	528 25–534 22	7.9	186(8)
1744–3922	0.172 444 360 995(2)	0.00 155(12)	525 30.0	36	519 53–531 07	0.3	148.1(7)
1750–2043	5.639 047 079(3)	7.9(16)	529 23.0	18	527 39–531 07	6.2	239(7)
1751–2857	0.0039 148 731 963 690(6)	0.0000 1126(4)	525 60.0	168	518 08–533 12	0.029	42.808(20)
1753–1914	0.0629 548 889 725(12)	0.00 202(12)	531 50.0	62	528 28–534 71	0.8	105.3(3)
1754–3510	0.392 703 893 399(3)	0.7816(5)	530 97.0	43	527 33–534 61	0.4	82.3(3)
1755–1650	0.73 374 443 871(3)	0.686(3)	531 65.0	55	528 60–534 71	1.1	159.9(10)
1756–2251	0.02 846 158 845 494(2)	0.0010 171(2)	520 86.0	1597	509 97–531 76	0.042	121.18(2)
1758–2846	0.76 670 638 621(3)	0.094(18)	532 53.0	39	530 63–534 43	1.3	66.6(3)
1759–1736	0.79 845 156 695(8)	0.255(20)	531 56.0	18	528 54–534 58	1.7	206(3)
1801–1417	0.0036 250 966 601 209(18)	0.00 000 531(11)	531 56.0	89	525 69–537 43	0.021	57.21(4)
1801–3458	1.3856 036 231(3)	0.4(4)	531 12.0	27	528 27–533 97	4.5	146(6)
1802–2124	0.012 647 593 582 763(5)	0.000 072(1)	528 55.0	30	526 05–531 05	0.007	149.6(1)
1805–1504	1.1812 692 298(3)	0.27(3)	530 35.0	58	525 99–534 71	14.2	225(3)
1808–1020	0.596 993 202 504(4)	0.7725(4)	530 35.0	63	525 99–534 71	0.5	225.3(8)
1808–1726	0.24 103 454 795(9)	<0.012	531 08.0	67	527 44–534 71	23.2	536(7)
1808–2701	2.45 788 177 758(12)	65.818(11)	531 12.0	56	527 51–534 72	2.6	95(4)
1811–2439	0.415 812 941 402(11)	0.2972(11)	531 65.0	54	528 59–534 71	0.9	172.0(5)
1812–2526	0.315 835 048 197(8)	0.1775(9)	531 71.0	54	528 71–534 71	1.1	361.4(4)
1814–0618	1.37 786 849 563(14)	0.292(16)	530 95.0	66	527 18–534 71	5.7	168(6)
1816–0755	0.2176 426 911 444(15)	6.48 032(15)	530 35.0	60	525 99–534 71	0.5	116.8(4)
1817–0743	0.438 095 346 909(18)	<0.0083	528 87.0	13	526 67–531 07	0.7	14.8(4)
1819–1318	1.51 569 599 263(12)	0.6(3)	528 56.0	13	526 04–531 07	1.0	35.1(15)
1820–0509	0.337 320 795 791(3)	0.9323(3)	530 35.0	47	526 08–534 61	0.4	104.0(3)
1821–0256	0.414 111 049 843(14)	0.0372(14)	530 97.0	67	527 32–534 61	1.8	84.0(4)
1822–0848	0.834 839 272 621(14)	0.135(4)	531 15.0	229	527 49–534 81	1.5	186.3(7)
1824–0127	2.49 946 826 743(11)	3.911(11)	530 40.0	51	526 08–534 71	3.0	58.0(15)
1824–2233	1.16 174 310 971(3)	0.301(3)	531 65.0	52	528 59–534 71	0.8	156.5(12)
1824–2328	1.50 587 455 169(3)	1.74(3)	531 11.0	44	527 51–534 71	0.7	185(3)
1827–0750	0.270 502 039 371(3)	1.5446(8)	532 23.0	38	529 74–534 71	0.4	381(9)
1828–2119	0.514 523 069 504(14)	1.2668(14)	530 35.0	57	525 99–534 71	1.9	268.0(6)
1829+0000	0.199 147 397 053(8)	0.5249(8)	531 12.0	75	527 52–534 71	2.5	114.0(4)
1830–0052	0.34 569 803 402(5)	0.237(8)	532 76.0	17	530 63–53 489	0.8	220.4(9)
1830–0131	0.152 511 958 009(4)	2.106(4)	530 95.0	125	527 18–534 71	1.5	95.7(3)
1830–1414	0.77 149 252 038(6)	0.076(11)	522 65.0	19	520 03–525 28	1.5	393.6(14)
1831–0952	0.0672 668 461 152(14)	8.32 385(3)	524 12.0	124	513 02–535 23	2.0	247(5)
1832+0029	0.533 917 296(6)	1.51(20)	533 44.0	13	528 87–531 53	0.7	28.3(12)
1834–0031	0.329 531 922 488(6)	0.4486(6)	530 30.0	48	525 99–534 61	1.0	155.1(6)
1834–1855	1.46 565 577 133(7)	1.931(9)	531 08.0	40	527 44–534 71	1.8	185.2(12)
1835–0349	0.84 186 451 859(4)	3.058(4)	531 25.0	20	528 53–533 97	0.5	269.6(7)
1835–0944	0.145 346 822 521(15)	4.39(13)	536 63.9	14	535 25–538 02	0.5	277.2(5)
1835–0946	0.37 953 610 601(5)	0.043(31)	536 63.0	13	535 25–538 02	0.4	193.3(5)
1835–1548	0.67 048 566 238(9)	1.74(14)	531 40.0	21	528 56–534 25	3.1	327(6)
1836–1324	0.1787 563 517 731(16)	1.0366(10)	532 77.0	41	530 83–534 71	0.2	157.33(10)

4 THE GALACTIC PULSAR POPULATION

To date, the total number of pulsars discovered by the Parkes multi-beam (hereafter PMB) survey is 742. This substantial haul, together with a further 11 transient radio sources found in the survey data associated with rotating neutron stars (McLaughlin et al. 2006), means that our survey is a phenomenal new probe of the Galactic neutron-star population. We also make use of the recently published

high-latitude pulsar survey of the region $-140^\circ < l < -100^\circ$ and $|b| < 60^\circ$ (hereafter PH survey, Burgay et al. 2006). Since the PMB and PH surveys were carried out using the same observing system, the pulsars detected represent a reasonably homogeneous sample from which to proceed.

Although the total number of pulsars detected by the PMB and PH surveys is 1055, for this analysis, where we are concerned with the properties of normal pulsars, we use only those 1008 non-binary

Table 2 – continued

PSR J	Period, P (s)	\dot{P} (10^{-15})	Epoch (MJD)	N_{TOA}	Data Span (MJD)	Residual (ms)	DM (cm^{-3} pc)
1837+0053	0.47 351 252 978(4)	0.038(4)	530 94.0	25	526 94–534 94	2.8	124(3)
1839–0436	0.149 460 655 762(3)	0.8096(3)	531 90.0	29	528 87–534 93	0.5	292.7(18)
1839–1238	1.91 142 802 251(5)	4.947(4)	530 35.0	46	525 99–534 71	1.4	169.8(18)
1840+0214	0.79 747 807 530(4)	8.294(7)	531 29.0	19	528 60–533 97	0.5	182.4(10)
1840–0840	5.3 093 766 847(20)	23.7(12)	532 78.0	39	530 84–534 71	9.3	272(19)
1840–1207	0.754 470 427 192(6)	3.1972(6)	530 38.0	57	526 04–534 71	0.5	302.3(15)
1841+0130	0.0297 727 753 332(4)	0.00 817(5)	531 11.0	155	527 49–534 72	0.7	125.88(6)
1841–1404	1.3345 572 305(8)	0.64(18)	531 73.0	21	528 56–534 91	5.9	267(8)
1842+0257	3.08 825 579 295(13)	29.591(12)	530 40.0	44	526 08–534 71	2.3	148.1(11)
1842+0358	0.233 326 206 679(3)	0.8115(3)	531 08.0	56	527 44–534 71	0.5	109.9(4)
1842+0638	0.313 016 401 038(11)	0.076(17)	531 25.0	18	528 54–533 97	0.4	212.2(12)
1843–1507	0.583 550 377 362(5)	7.1999(6)	530 95.0	49	527 18–534 71	0.5	215.5(7)
1845+0623	1.42 165 378 409(7)	0.546(7)	530 95.0	42	527 18–534 71	1.8	113.0(14)
1845–0826	0.634 354 346 767(17)	9.353(3)	531 12.0	40	527 52–534 71	1.3	228.2(12)
1845–1114	0.2062 199 811 321(13)	2.00 552(13)	530 36.0	58	525 99–534 72	0.4	206.7(5)
1845–1351	2.61 891 846 726(6)	9.723(8)	531 12.0	39	527 51–534 72	1.2	197.4(14)
1846–0749	0.350 109 572 852(4)	1.2616(4)	531 72.0	51	528 71–534 72	0.3	388.3(5)
1848–0601	0.225 004 475 404(4)	0.2871(4)	530 41.0	48	526 09–534 72	1.0	496.6(4)
1848–1150	1.31 221 843 801(3)	1.434(3)	530 40.0	51	526 08–534 72	1.5	163.4(18)
1849+0409	0.761 194 081 655(11)	21.5864(12)	530 35.0	41	526 08–534 61	0.8	56.1(14)
1851–0114	0.95 318 168 518(4)	2.483(4)	530 38.0	48	526 04–534 72	2.2	427.2(14)
1853+0853	3.9146 579 157(5)	5.13(7)	530 97.0	17	527 39–534 55	2.9	214(5)
1853+1303	0.0040 917 973 806 819(14)	0.00 000 885(10)	529 72.0	140	526 06–533 37	0.003	30.5702(12)
1856–0526	0.370 483 417 429(7)	1.6975(9)	530 95.0	42	527 18–534 72	1.0	130.5(4)
1901–0315	0.80 169 309 688(11)	2.57(4)	532 83.0	22	530 75–534 91	1.0	242.6(16)
1901+0435	0.6905 763 581(3)	8.67(3)	530 41.0	118	526 00–534 81	33.8	1042.6(10)
1901+0621	0.83 200 194 892(5)	0.018(3)	522 82.0	21	514 58–531 06	4.2	94(7)
1903–0258	0.301 458 774 079(6)	0.6791(6)	530 95.0	49	527 18–534 72	0.9	113.0(5)
1903+0925	0.35 715 482 026(9)	36.899(13)	533 96.0	17	530 50–537 42	6.3	162(6)
1904–0150	0.379 387 161 967(6)	0.8898(8)	531 07.0	34	527 52–534 61	0.5	162.2(5)
1906+0414	1.043 361 628 655(9)	11.461(9)	536 77.0	8	535 53–538 02	0.014	349(9)
1907+1149	1.42 016 034 143(17)	159.79(3)	534 45.0	26	531 48–537 42	3.2	202.8(15)
1910–0112	1.3606 029 280(8)	0.18(6)	531 74.0	15	528 61–534 87	8.6	178(26)
1910+1256	0.0049 835 839 397 055(12)	0.00 000 977(7)	529 70.0	183	526 02–533 37	0.002	38.0650(7)
1911+1347	0.0046 259 624 652 639(15)	0.00 001 712(20)	530 94.0	59	527 18–534 71	0.020	30.99(5)
1913+0904	0.163 245 785 775(11)	17.6167(8)	532 49.0	23	530 04–534 94	0.1	95.3(6)
1914+0219	0.457 526 573 507(11)	1.0181(4)	530 40.0	66	526 08–534 72	0.6	233.8(4)
1915+0227	0.3173 062 332 319(16)	0.29 898(15)	530 36.0	56	526 00–534 72	0.4	192.6(5)
1915+1410	0.297 494 121 670(7)	0.0489(8)	533 99.0	20	530 55–537 42	0.5	273.7(3)
1921+0812	0.2106 484 121 028(14)	5.3633(6)	532 77.0	39	530 83–534 71	0.1	84.0(6)
1927+0911	0.290 305 256 197(5)	0.0635(4)	534 54.0	44	531 53–537 55	0.4	202.7(4)
1941+1341	0.559 084 099 229(13)	1.2387(13)	530 41.0	59	526 00–534 81	1.5	147.9(3)

pulsars with $P > 30$ ms. In this sample, 976 pulsars were detected solely by the PMB survey, 22 were detected solely by the PH survey and 12 were detected jointly. While there are two additional large-scale surveys using the Parkes multibeam system (Edwards et al. 2001; Jacoby 2005), these are not included at this stage of the analysis due to lack of flux densities for many of the pulsars from these surveys. However, these surveys are utilized later in the discussion (Section 4.5.2) when the scaleheight of the population is investigated.

In the following, we investigate various aspects of the Galactic pulsar population after accounting, as far as possible, for the known selection effects. We begin by presenting a model for the survey detection process which is in good agreement with the observed S/N s from the PMB survey. We then use this detection model in a Monte

Carlo simulation to iteratively deduce various underlying Galactic population properties. Finally, we apply a pulsar current analysis on our optimal model to deduce the birth rate of the population.

4.1 Survey detection model

Although Manchester et al. (2001) presented a detailed formalism to calculate the survey sensitivity, we have found that a simpler approach is to use the radiometer equation (see, e.g. Dewey et al. 1984). As we show below this provides a self-consistent model for the detection statistics. This approach was also adopted by Faucher-Giguère & Kaspi (2006) where it was noted that there appears to be some inconsistencies with the procedure given by Manchester et al. (2001). The radiometer equation gives the observed S/N in terms

Table 3. Derived parameters for 142 pulsars discovered in this phase of the Parkes multibeam pulsar survey. Listed are the base-10 logarithms of characteristic age (yr), the surface dipole magnetic field strength (G), the loss in rotational energy (erg s^{-1}), the DM-derived distance using the Taylor & Cordes (1993) model, D_{TC} (kpc), and the Cordes & Lazio (2002) model, D_{CL} (kpc), the corresponding z heights, z_{TC} and z_{CL} (both in kpc) and the inferred radio luminosity at 1400 MHz for each distance estimate L_{TC} and L_{CL} (both in mJy kpc^2).

PSR J	$\log[\tau_c]$	$\log[B]$	$\log[\dot{E}]$	D_{TC}	D_{CL}	z_{TC}	z_{CL}	L_{TC}	L_{CL}
0733–2345	6.70	12.51	31.59	12.03	8.04	−0.43	−0.28	10.1	4.5
0932–5327	6.92	12.79	30.59	3.91	2.31	−0.09	−0.06	2.3	0.8
1001–5939	6.31	13.34	30.71	3.31	2.76	−0.20	−0.17	1.6	1.1
1020–6026	5.52	11.99	34.98	30.00	12.19	−1.49	−0.61	126.0	20.8
1107–5907	8.65	10.68	31.34	1.81	1.28	0.04	0.02	0.6	0.3
1125–6014	10.02	8.02	33.94	1.94	1.50	0.03	0.02	0.2	0.1
1148–5725	6.71	12.80	30.99	6.95	3.75	0.54	0.29	5.8	1.7
1216–6410	10.54	7.88	33.15	1.71	1.33	−0.05	−0.04	0.1	0.1
1308–5844	5.93	12.31	33.53	8.92	4.59	0.63	0.32	16.7	4.4
1355–5747	7.66	12.09	30.52	7.57	5.08	0.53	0.36	20.6	9.3
1357–6429	3.86	12.89	36.49	4.03	2.47	−0.18	−0.11	7.1	2.7
1405–5641	6.91	11.94	32.30	21.25	6.73	1.76	0.56	45.2	4.5
1439–5501	9.51	9.31	32.38	0.76	0.60	0.06	0.05	0.2	0.2
1519–5734	6.28	12.18	33.08	13.07	8.81	−0.05	−0.04	76.9	34.9
1519–6106	6.61	12.63	31.52	7.18	4.35	−0.40	−0.24	9.8	3.6
1538–5732	6.08	12.10	33.65	3.88	2.83	−0.11	−0.08	5.3	2.8
1558–5756	4.98	13.16	33.72	3.74	2.50	−0.23	−0.16	2.7	1.2
1600–5916	7.35	12.03	31.26	6.47	3.73	−0.54	−0.31	13.8	4.6
1604–4718	6.23	12.21	33.11	1.48	2.14	0.10	0.14	0.5	1.0
1611–5847	9.45	10.43	30.26	2.32	1.70	−0.22	−0.16	0.6	0.3
1617–4608	5.74	12.49	33.56	10.98	6.07	0.60	0.33	18.1	5.5
1622–4347	6.16	12.19	33.32	5.42	3.51	0.40	0.26	5.3	2.2
1624–4411	6.66	11.64	33.40	3.66	2.70	0.23	0.17	6.4	3.5
1624–4613	>8.06	<11.51	<30.86	5.18	3.76	0.20	0.15	10.5	5.5
1627–4706	6.11	11.70	34.40	7.34	6.03	0.16	0.13	5.4	3.6
1631–4155	9.00	10.85	30.32	8.60	4.81	0.65	0.36	14.1	4.4
1634–5107	6.71	11.96	32.68	9.20	6.09	−0.37	−0.24	29.6	13.0
1637–4450	6.84	11.59	33.15	8.80	6.49	0.23	0.17	31.0	16.8
1638–3815	8.16	11.37	30.95	17.25	5.66	1.73	0.57	184.5	19.9
1638–4725	6.40	12.29	32.62	6.73	6.07	−0.04	−0.03	14.5	11.8
1643–4505	5.07	12.44	34.97	6.37	5.64	0.06	0.05	11.4	8.9
1646–5123	6.60	12.03	32.75	10.62	5.63	−0.73	−0.39	19.2	5.4
1649–3805	8.05	11.00	31.90	6.89	4.30	0.50	0.31	47.5	18.5
1650–4921	6.13	11.73	34.28	5.77	4.08	−0.31	−0.22	5.3	2.7
1653–4030	7.57	11.83	31.20	10.94	6.68	0.40	0.25	47.9	17.8
1654–3710	7.31	11.92	31.54	14.10	6.33	0.99	0.44	43.7	8.8
1656–3621	6.96	11.99	32.11	7.85	4.67	0.58	0.35	17.9	6.3
1700–3611	6.74	12.41	31.71	6.80	4.48	0.44	0.29	23.6	10.2
1700–4012	7.66	11.23	32.23	5.94	5.07	0.13	0.11	4.6	3.3
1711–4322	7.79	10.72	32.99	4.15	3.83	−0.16	−0.15	4.5	3.8
1715–3859	6.52	12.31	32.34	10.32	9.34	−0.06	−0.06	57.5	47.1
1717–3953	8.72	11.28	30.00	6.68	5.65	−0.14	−0.11	34.8	24.9
1718–4539	6.10	12.33	33.15	10.69	6.35	−0.85	−0.51	9.1	3.2
1722–4400	6.97	11.46	33.15	7.02	5.14	−0.53	−0.39	10.8	5.8
1724–4500	6.77	12.34	31.79	6.15	4.56	−0.55	−0.41	1.9	1.0
1725–2852	7.00	12.20	31.60	4.09	3.13	0.27	0.21	4.2	2.4
1728–4028	7.77	11.66	31.15	5.40	4.08	−0.30	−0.23	20.1	11.5
1730–2900	6.44	12.57	31.98	6.97	5.04	0.34	0.25	6.3	3.3
1732–3426	7.12	11.57	32.63	6.35	5.74	−0.06	−0.05	9.7	7.9
1733–2533	6.70	12.08	32.46	8.01	5.00	0.57	0.36	6.4	2.5

of various pulsar and system parameters as follows:

$$S/N = S_{1400} G \frac{\sqrt{n_p \Delta \nu \tau}}{\beta T} \sqrt{\frac{P - W}{W}}. \quad (1)$$

Here S_{1400} is the pulsar mean flux density at 1400 MHz (mJy), G is the effective telescope gain (K/Jy), n_p is the number of polarizations summed, $\Delta \nu$ is the observing bandwidth (MHz), τ is the integration time (s), β accounts for S/N losses, T is the system temperature (K),

Table 3 – continued

PSR J	$\log[\tau_c]$	$\log[B]$	$\log[\dot{E}]$	D_{TC}	D_{CL}	z_{TC}	z_{CL}	L_{TC}	L_{CL}
1733–2837	7.04	11.97	31.98	4.72	3.87	0.20	0.16	1.6	1.0
1734–2415	6.97	11.91	32.26	3.51	2.59	0.28	0.21	3.6	1.9
1736–2457	7.09	12.48	30.86	4.46	3.38	0.29	0.22	10.3	5.9
1738–2330	6.56	12.62	31.64	2.79	2.05	0.21	0.15	3.7	2.0
1739–3951	8.44	10.92	31.30	1.13	0.78	−0.09	−0.06	0.2	0.1
1741–2719	7.83	11.23	31.88	5.99	5.28	0.17	0.15	7.2	5.6
1742–3957	8.29	11.46	30.49	6.40	3.90	−0.57	−0.35	5.7	2.1
1744–3922	9.25	10.22	31.08	4.60	3.06	−0.41	−0.27	4.2	1.9
1750–2043	7.05	12.83	30.26	5.81	4.84	0.34	0.28	8.1	5.6
1751–2857	9.74	8.33	33.87	1.44	1.10	−0.03	−0.02	0.1	0.1
1753–1914	8.69	10.06	32.51	2.80	2.17	0.17	0.13	1.0	0.6
1754–3510	6.90	11.75	32.71	2.22	1.95	−0.19	−0.17	2.3	1.8
1755–1650	7.23	11.86	31.84	4.31	3.40	0.32	0.25	2.4	1.5
1756–2251	8.65	9.74	33.23	2.92	2.48	0.05	0.04	5.1	3.7
1758–2846	8.11	11.43	30.91	1.71	1.76	−0.07	−0.07	0.6	0.6
1759–1736	7.70	11.66	31.30	4.83	4.00	0.26	0.21	2.8	1.9
1801–1417	10.03	8.15	33.64	1.80	1.52	0.13	0.11	0.6	0.4
1801–3458	7.74	11.88	30.77	4.88	3.49	−0.51	−0.37	2.6	1.3
1802–2124	9.44	8.98	33.15	3.33	2.94	0.04	0.03	8.5	6.7
1805–1504	7.84	11.76	30.82	5.33	4.38	0.29	0.24	62.5	42.2
1808–1020	7.09	11.84	32.15	8.95	5.29	0.72	0.42	18.4	6.4
1808–1726	8.52	10.73	31.52	9.45	7.85	0.20	0.16	34.8	24.0
1808–2701	5.77	13.11	32.23	2.43	1.71	−0.14	−0.10	0.9	0.4
1811–2439	7.35	11.55	32.20	3.79	3.62	−0.20	−0.19	3.7	3.4
1812–2526	7.45	11.38	32.34	13.76	8.00	−0.83	−0.48	34.1	11.5
1814–0618	7.87	11.81	30.64	5.86	4.22	0.53	0.38	19.9	10.3
1816–0755	5.73	12.08	34.40	3.24	2.78	0.23	0.20	1.8	1.3
1817–0743	>8.92	<10.79	<30.59	0.77	0.80	0.05	0.05	0.1	0.2
1819–1318	7.60	11.98	30.83	1.52	1.15	0.02	0.02	0.4	0.2
1820–0509	6.76	11.75	32.98	2.84	2.51	0.22	0.20	2.0	1.6
1821–0256	8.25	11.10	31.32	2.55	2.36	0.24	0.22	1.2	1.1
1822–0848	7.99	11.53	30.96	4.24	3.77	0.17	0.15	0.7	0.6
1824–0127	7.00	12.50	31.00	2.21	1.88	0.20	0.17	2.9	2.1
1824–2233	7.79	11.78	30.88	4.22	3.78	−0.33	−0.29	3.9	3.1
1824–2328	7.14	12.21	31.30	5.61	4.55	−0.48	−0.39	10.1	6.6
1827–0750	6.44	11.82	33.49	7.45	6.04	0.23	0.19	77.7	51.1
1828–2119	6.81	11.91	32.57	12.06	6.77	−0.99	−0.56	55.3	17.4
1829+0000	6.78	11.51	33.41	3.40	3.22	0.29	0.27	5.0	4.5
1830–0052	7.36	11.46	32.36	7.37	5.68	0.55	0.42	2.2	1.3
1830–0131	6.06	11.76	34.36	2.69	2.66	0.19	0.19	2.5	2.5
1830–1414	8.20	11.39	30.81	7.80	6.26	−0.25	−0.20	6.1	3.9
1831–0952	5.11	11.88	36.04	4.32	4.04	−0.01	−0.01	6.2	5.4
1832+0029	6.75	11.96	32.59	1.45	1.32	0.11	0.10	0.3	0.2
1834–0031	7.06	11.59	32.69	4.47	3.96	0.27	0.24	3.4	2.7
1834–1855	7.08	12.23	31.38	5.95	4.62	−0.52	−0.40	17.0	10.2
1835–0349	6.64	12.21	32.30	5.27	5.59	0.17	0.18	4.4	5.0
1835–0944	5.72	11.91	34.75	4.63	4.37	−0.08	−0.08	8.8	7.8
1835–0946	8.14	11.11	31.49	4.02	3.61	−0.07	−0.06	2.9	2.3
1835–1548	6.79	12.04	32.36	13.52	7.51	−0.89	−0.50	11.0	3.4
1836–1324	6.44	11.64	33.86	3.87	3.48	−0.20	−0.18	1.5	1.2

P is the pulse period (s) and W is the observed pulse width (s). Since both the PMB and PH surveys used the same telescope, receiver and data acquisition system, the only parameter that is different is the integration time $\tau = 2097$ s for the PMB survey and 262 s for the PH survey. The constant parameters are $n_p = 2$, $\Delta\nu = 288$ MHz and $\beta = \sqrt{\pi/2} \simeq 1.25$ for S/N losses due to one bit digitization (see e.g. Lorimer & Kramer 2005). Gain and system

temperature values depend primarily on which element of the 13-beam receiver system was used to make the detection. We use the values given by Manchester et al. (2001). Sky temperature values vary as a function of Galactic latitude and longitude. To account for this, we use the Haslam et al. (1982) 430-MHz all-sky catalogue scaled to the observing frequency of 1400 MHz assuming a sky background spectral index of -2.6 (Lawson et al. 1987).

Table 3 – *continued*

PSR J	$\log [\tau_c]$	$\log [B]$	$\log [\dot{E}]$	D_{TC}	D_{CL}	z_{TC}	z_{CL}	L_{TC}	L_{CL}
1837+0053	8.30	11.13	31.15	3.27	3.41	0.20	0.21	3.6	4.0
1839-0436	6.47	11.55	33.98	4.98	5.45	0.06	0.06	5.7	6.8
1839-1238	6.79	12.49	31.45	4.13	3.74	-0.23	-0.21	6.3	5.2
1840+0214	6.18	12.41	32.81	5.50	4.93	0.33	0.30	2.1	1.7
1840-0840	6.55	13.05	30.79	4.84	4.82	-0.14	-0.14	23.4	23.2
1840-1207	6.57	12.20	32.46	8.82	6.13	-0.49	-0.34	17.1	8.3
1841+0130	7.76	10.20	34.08	3.20	3.59	0.16	0.18	0.6	0.8
1841-1404	7.52	11.97	31.04	10.42	6.36	-0.77	-0.47	19.5	7.3
1842+0257	6.22	12.99	31.60	4.00	4.26	0.23	0.25	4.2	4.7
1842+0358	6.66	11.64	33.40	3.21	3.53	0.22	0.24	0.9	1.1
1842+0638	7.81	11.19	31.99	11.23	6.80	0.99	0.60	26.5	9.7
1843-1507	6.11	12.32	33.15	8.71	5.52	-0.78	-0.49	12.9	5.2
1845+0623	7.62	11.95	30.88	3.53	3.86	0.27	0.29	4.1	4.9
1845-0826	6.03	12.39	33.15	4.86	4.48	-0.21	-0.19	7.8	6.6
1845-1114	6.21	11.81	33.95	5.54	4.52	-0.37	-0.30	16.0	10.6
1845-1351	6.63	12.71	31.32	7.01	4.95	-0.60	-0.42	16.2	8.1
1846-0749	6.64	11.83	33.08	9.82	7.16	-0.42	-0.30	33.8	17.9
1848-0601	7.09	11.41	33.00	11.55	9.52	-0.41	-0.34	32.0	21.8
1848-1150	7.16	12.14	31.40	4.73	3.98	-0.38	-0.32	4.7	3.3
1849+0409	5.75	12.61	33.28	2.41	2.42	0.10	0.10	0.6	0.6
1851-0114	6.78	12.19	32.04	6.26	6.90	-0.06	-0.06	11.0	13.3
1853+0853	7.08	12.66	30.53	7.67	6.75	0.48	0.43	6.5	5.0
1853+1303	9.87	8.29	33.71	1.60	2.05	0.15	0.19	1.0	1.7
1856-0526	6.54	11.90	33.11	3.41	3.32	-0.21	-0.21	4.7	4.4
1901-0315	6.69	12.16	32.30	6.84	5.94	-0.44	-0.38	4.2	3.2
1901+0435	6.10	12.39	33.00	30.00	19.07	-0.08	-0.05	243.0	98.2
1901+0621	8.86	11.09	30.08	3.11	3.40	0.04	0.05	4.5	5.4
1903-0258	6.85	11.66	32.99	3.07	3.16	-0.22	-0.22	1.3	1.4
1903+0925	5.18	12.56	34.51	4.20	4.95	0.11	0.13	3.5	4.9
1904-0150	6.83	11.77	32.81	4.77	4.36	-0.32	-0.29	2.0	1.7
1906+0414	6.16	12.54	32.60	9.24	7.50	-0.24	-0.20	19.6	12.9
1907+1149	5.15	13.18	33.34	5.33	5.98	0.17	0.19	3.7	4.6
1910-0112	8.08	11.70	30.45	6.36	5.03	-0.53	-0.42	2.8	1.8
1910+1256	9.91	8.35	33.49	1.95	2.32	0.06	0.07	1.9	2.7
1911+1347	9.63	8.45	33.83	1.60	2.07	0.05	0.07	0.2	0.3
1913+0904	5.17	12.24	35.20	3.48	2.85	-0.04	-0.03	0.8	0.6
1914+0219	6.85	11.84	32.62	9.57	6.98	-0.67	-0.49	68.7	36.5
1915+0227	7.23	11.49	32.57	7.00	5.89	-0.50	-0.42	27.0	19.1
1915+1410	7.98	11.09	31.86	7.81	7.93	0.16	0.17	6.1	6.3
1921+0812	5.79	12.03	34.36	3.44	3.46	-0.18	-0.18	7.8	7.9
1927+0911	7.86	11.14	32.00	7.05	6.75	-0.45	-0.44	8.0	7.3
1941+1341	6.85	11.93	32.45	8.52	5.50	-0.66	-0.43	12.3	5.1

To account for the drop in flux density away from the beam centre, we can assume a Gaussian beam (see e.g. Lorimer et al. 1993) to write

$$G = G_0 \exp\left(\frac{-2.77r^2}{w^2}\right), \quad (2)$$

where G_0 is the telescope gain at the beam centre, r is the offset from the beam centre and w is the full width at half power of the telescope beam. For each detection under consideration, we adopt the G_0 and w values given by Manchester et al. (2001) for the appropriate beam of the multibeam receiver when making this correction. To calculate the equivalent pulse width W from the observed 50 per cent width, W_{50} , we make a simplification that the pulse shape is Gaussian in form (a reasonable approximation for most pulsars). For a Gaussian pulse with an intensity of unity and a standard deviation σ , we find

that $W_{50} = \sigma\sqrt{8\ln 2}$ and W is just the area under the pulse (i.e. $W = \sigma\sqrt{2\pi}$). Eliminating σ from these two equalities yields the relationship

$$W = W_{50} \sqrt{\frac{\pi}{4\ln 2}} \simeq 1.06W_{50}. \quad (3)$$

Fig. 2 shows a comparison between the modelled and observed S/N values using the data taken from Table 1 and the corresponding data from the earlier papers in this series. The error bars are derived directly from the uncertainties in the measured flux densities of each pulsar. As can be seen, the agreement between our model and observed S/N values is good, being largely free from systematic trends and with a scatter that is not much larger than the uncertainties. In addition to providing a sanity check on the system

Table 4. Summary of the 13 binary pulsars discovered in this phase of the Parkes multibeam survey. For each system, we give the spin period (P), orbital period (P_b), projected semimajor axis (x) and orbital eccentricity (e). The right-hand column gives the source of the more detailed parameters which refer to either external papers or additional tables below.

PSR	P (ms)	P_b (d)	x (light-second)	e	Further details
J1125–6014	2.63	8.75	8.34	7.9×10^{-7}	Table 6
J1216–6410	3.54	4.04	2.94	6.8×10^{-6}	Table 6
J1439–5501	28.6	2.12	9.84	5.0×10^{-5}	Table 6
J1638–4725	764	1940	2380	0.95	Lyne et al. (in preparation)
J1711–4322	103	922	140	2.4×10^{-3}	Table 5
J1744–3922	172	0.191	0.212	1.3×10^{-3}	Faulkner et al. (2004)
J1751–2857	3.92	111	32.5	1.3×10^{-4}	Stairs et al. (2005)
J1756–2251	28.5	0.320	2.76	0.18	Faulkner et al. (2005)
J1802–2124	12.6	0.699	3.72	3.2×10^{-6}	Faulkner et al. (2004)
J1822–0848	835	287	97.8	0.059	Table 5
J1841+0130	29.8	10.5	3.50	8.2×10^{-5}	Table 6
J1853+1303	4.09	116	40.8	2.4×10^{-5}	Stairs et al. (2005)
J1910+1256	4.98	58.5	21.1	2.3×10^{-4}	Stairs et al. (2005)

Table 5. Orbital parameters for the two binary pulsars obtained using the Blandford & Teukolsky (1976) binary model. The minimum companion mass is calculated by assuming an inclination angle of 90° and a neutron star mass of $1.35 M_\odot$. Figures in parentheses represent 1σ uncertainties in the least significant digit(s).

PSR	J1711–4322	J1822–0848
Orbital period (d)	922.4707(7)	286.8303(14)
Projected semimajor axis of orbit (light-second)	139.6245(6)	97.7279(20)
Eccentricity	0.002 375(6)	0.058 962(9)
Epoch of periastron (MJD)	50 208.8(3)	52 672.848(9)
Longitude of periastron ($^\circ$)	293.75(12)	272.583(10)
Mass function (M_\odot)	0.00 343 446(2)	0.0121 811(3)
Minimum companion mass (M_\odot)	0.20	0.32

performance, this analysis demonstrates that equation (1) provides a good model of the survey detection thresholds and, for the sample of normal pulsars presented here, we recommend its use in future analyses.

4.2 Galactic distribution determination method

Using the above model for the PMB and PH surveys, we now describe a method to derive the underlying probability density functions (PDFs) in pulse period (P), 1400-MHz radio luminosity (L), Galactocentric radius (R) and height above the Galactic plane (z). The modelling technique we use is based on the iterative procedure developed by Large (1971), Taylor & Manchester (1977) and Lyne, Manchester & Taylor (1985). A preliminary account of the analysis below was presented by Lorimer (2004).

Our goal is to produce a model of the Galactic pulsar population which, when filtered through the above survey detection models of the PMB and PH surveys, produces a set of ‘model detectable pulsars’ which closely matches the observed sample. A Monte Carlo simulation package⁵ was developed for this work and is freely available for checking the results presented here, and for further use.

We simulate the Galactic pulsar distribution by drawing pulsars from independent numerical PDFs in R , z , L and P . The justification for assuming no correlation between the distributions is twofold. First, no statistically significant correlations between these parameters exist in the known sample (Lorimer 2004). Secondly, our modelling philosophy is to create a *snapshot of the currently observable pulsar population*, rather than attempting to follow the time evolution (see e.g. Faucher-Giguère & Kaspi 2006, and references therein). Although there are advantages to taking the time-evolution approach, particularly when investigating the evolution of pulsar luminosities and magnetic field strengths, we prefer to adopt the simpler procedure here which concentrates on issues relating to the present-day spatial, period and luminosity distributions.

We choose the four numerical PDFs as follows: for the R distribution we consider 15 equal zones between 0 and 15 kpc; for the z distribution we consider 31 equal zones between -1.5 and 1.5 kpc; for the L distribution we consider 12 logarithmically spaced zones between 0.1 and 1000 mJy kpc² each one third of a decade wide; for the P distribution we consider 15 logarithmically spaced zones between 30 ms and 10 s each one sixth of a decade wide. To begin with, we assume no prior knowledge and distribute pulsars completely uniformly in space and use flat PDFs in $\log L$ and $\log P$. We also experimented with other starting PDFs and concluded that any function which reasonably samples the parameter range produces results that are consistent with those found below.

During the course of this work, we found that the most important factor limiting our determination of the true spatial density of pulsars in the Galaxy was the uncertainty in the Galactic distribution of free electrons. We therefore distinguish between two different models. The first model (hereafter referred to as ‘S’ for smooth), treats the pulsar and free electron density distributions as smooth and azimuthally symmetric functions with respect to the Galactic Centre. The second model (hereafter referred to as ‘C’ for clumpy), attempts to incorporate Galactic spiral-arm structure and a heterogeneous distribution of free electrons.

To specify the location of any model pulsar, we use a Cartesian (x , y , z) coordinate system where the Galactic Centre is at the origin, and the Sun is at (0.0, 8.5, 0.0) kpc. With this definition $R = \sqrt{x^2 + y^2}$. For a given pair of R and z values, then, we can calculate the Cartesian coordinates of each model pulsar. We achieve this in two different ways. In model S, we choose a random

⁵<http://psrpop.sourceforge.net>

Table 6. Orbital parameters for the four binary pulsars obtained using the ‘ELL1’ binary timing model (Lange et al. 2001), where the first and second Laplace–Lagrange parameters are defined by $e \cos \omega$ and $e \sin \omega$, respectively (for an orbital eccentricity e and longitude of periastron ω). The minimum companion mass is calculated by assuming an inclination angle of 90° and a neutron star mass of $1.35 M_\odot$. Figures in parentheses represent 1σ uncertainties in the least significant digit(s).

PSR	J1125–6014	J1216–6410	J1439–5501	J1841+0130
Orbital period (d)	8.75 260 353(5)	4.03 672 718(6)	2.117 942 520(3)	10.471 626(5)
Projected semimajor axis of orbit (light-second)	8.339 198(5)	2.937 091(7)	9.833 404(7)	3.50 409(18)
First Laplace–Lagrange parameter	–0.0000 008(13)	0.0000 004(60)	–0.0000 495(15)	–0.0000 033(10)
Second Laplace–Lagrange parameter	0.00 000 005(120)	–0.000 007(6)	0.0000 059(13)	–0.00 008(10)
Epoch of ascending node (MJD)	53 171.5856 408(11)	53 055.3611 070(20)	53 058.0499 527(3)	52 747.55 445(11)
Mass function (M_\odot)	0.008 127 952(7)	0.00 1669 461(6)	0.2275 967(2)	0.00 042 129(3)
Minimum companion mass (M_\odot)	0.28	0.16	1.11	0.096

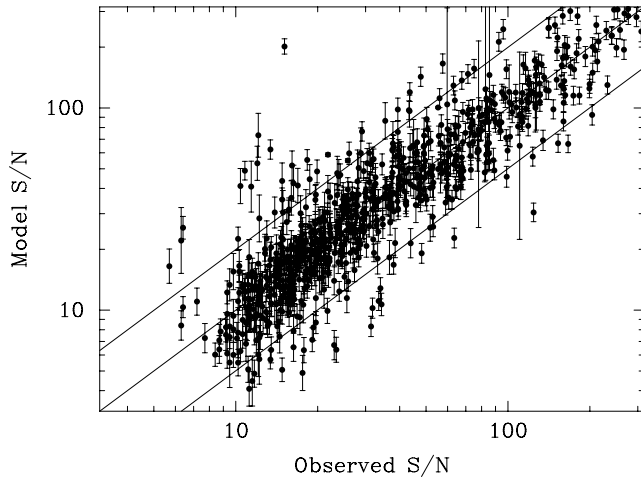


Figure 2. Model versus observed S/N ratios calculated as described in Section 4.1. The central diagonal line shows equality between theory and observation, while the outer lines show the range of a factor of 2. Uncertainties in the model S/N values are calculated directly from the uncertainties in the observed flux densities.

azimuthal angle in the disc of the galaxy θ from a flat PDF in the range $0 \leq \theta \leq 2\pi$. The coordinates are then simply $x = R \sin \theta$ and $y = R \cos \theta$. In model C, we follow the procedure described by Faucher-Giguère & Kaspi (2006) to weight the pulsar distribution along model spiral arms and calculate the appropriate x and y positions. In both cases, after determining the x , y and z coordinates of each pulsar, it is straightforward to compute its true distance from the Sun d and apparent Galactic coordinates, l and b . Finally from the distance and luminosity of each pulsar, and the definition $L = S_{1400} d^2$, we calculate the true 1400-MHz flux density, S_{1400} .

As mentioned in the previous section, the true flux density needs to be corrected for the position offset between a pulsar and the nearest telescope pointing in the survey. The PMB survey comprises data from 40 077 beam positions shown in Fig. 3. Although the pointings principally cover the longitude range $-100^\circ < l < 50^\circ$ and $|b| < 5^\circ$, as can be seen there is some coverage of the region $-140^\circ < l < -100^\circ$ and $|b| < 3^\circ$. From the sky position of each model pulsar we use this data base to find the closest beam position in the survey. To model the PH survey, which had a total of 6456 beam positions in the region $-140^\circ < l < -100^\circ$ and $|b| < 60^\circ$, we randomly choose an offset within the full-width half power point of a telescope beam.

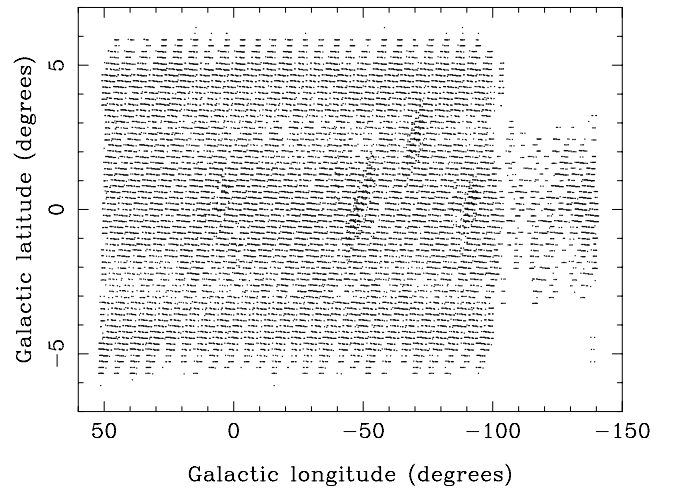


Figure 3. Distribution of observed beam positions in Galactic coordinates. Note that, for clarity, the size of each dot is much smaller than a beam width. The positions are spaced by the full-width half maximum and form an essentially uniform coverage of the region $-100^\circ < l < 50^\circ$. At lower longitudes, i.e. outside the main survey region, the coverage is incomplete. A file containing the exact sky positions shown here is available as part of the online version of this article, available at <http://www.blackwell-synergy.com> (Table S1).

From the corresponding position offset and true flux density, we use equation (2) to find the effective flux density, S .

To calculate DMs, we integrate two different models for the free electron density out along the appropriate line of sight defined by l and b until the distance d is reached. For model S we use the azimuthally symmetric and smooth model⁶ derived by Lyne et al. (1985), while for model C, we adopt the free electron distribution due to Cordes & Lazio (2002) which attempts to account for the clumpy nature of the interstellar medium including spiral-arm structure. As discussed by Lyne et al. (1985) and Cordes & Lazio (2002), the overall random errors in both models result in distance uncertainties of the order of 20 per cent. We account for this in both models by dithering all true distances using a Gaussian distribution with a fractional error of 20 per cent and use the symbol $\hat{\cdot}$ to denote parameters affected by this distance uncertainty. Hence, in addition

⁶We note that a more recent electron density model proposed by Gómez, Benjamin & Cox (2001) was not used here due to its lack of predictive power for pulsars in the inner Galaxy ($R < 4$ kpc).

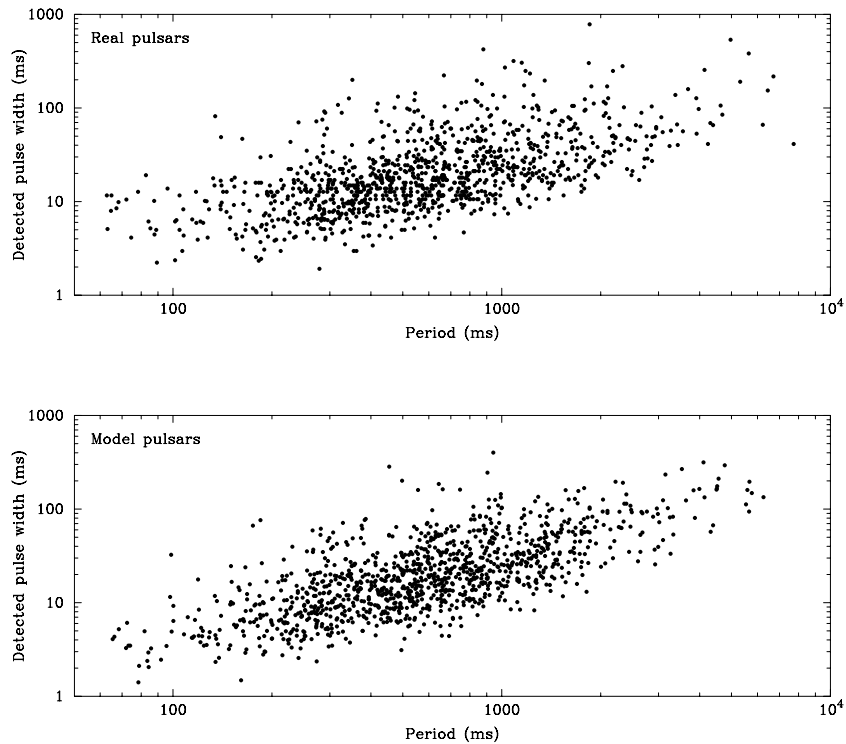


Figure 4. Distribution of observed pulse widths as a function of pulse period for the observed sample (top panel) and a model sample (bottom panel). The model pulsars were generated assuming an empirically derived correlation given in equation (5).

to the dithered distance, \hat{d} , we have $\hat{L} = S\hat{d}^2$, $\hat{R} = \sqrt{\hat{x}^2 + \hat{y}^2}$ and $\hat{z} = \hat{d} \sin b$ as the corresponding radius, R , and z -height estimates. For self-consistency, when comparing our model samples with the observations below, we use the model \hat{L} , \hat{R} and \hat{z} quantities.

Having computed the position and flux density of each pulsar, we are now in a position to model its detectability. To determine the model S/N using equation (1), we need to find the detected pulse width, W . This can be written in terms of the intrinsic pulse width W_{int} and a number of other factors in the following quadrature sum:

$$W = \sqrt{W_{\text{int}}^2 + W_{\text{DM}}^2 + t_{\text{samp}}^2 + t_{\text{scatt}}^2}. \quad (4)$$

Here W_{DM} is the dispersive broadening across individual filterbank channels, t_{samp} is the data sampling interval (multiples of 250 μs for the PMB survey and multiples of 125 μs for the PH survey) and t_{scatt} is the interstellar scattering time. In the following, we examine each of the quantities on the right-hand side of this equation in turn.

It is well known (see e.g. Lyne & Manchester 1988) that pulse widths are correlated with pulse period. During the course of this work, it became obvious that the observed scatter in the W - P plane (see Fig. 4) cannot be explained by a random relationship. Some correlation between W and P is to be expected, given the known variation in beam size with pulse period (see e.g. Biggs 1990), despite being blurred by an arbitrary viewing geometry for each pulsar. Rather than adopt a complicated beam model, we adopt a purely empirical approach in our simulations by assigning the intrinsic pulse width, W_{int} , as follows:

$$\log W_{\text{int}} = \log \left[0.06 \left(\frac{P}{\text{ms}} \right)^{0.9} \right] + \Gamma, \quad (5)$$

where Γ is a suitably normalized Gaussian distribution about the origin with a standard deviation of 0.3. These parameters were found

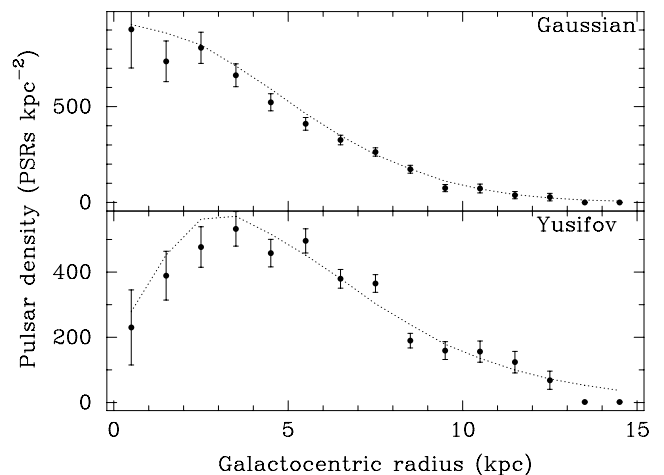


Figure 5. Underlying (dotted lines) and derived (points) radial density functions run for two tests of the Galactic distribution determination. The top panel shows an input population with a Gaussian radial profile, while the lower panel shows a population generated using the radial density profile of Yusifov & Küçük (2004) (see Section 4.3).

by experimentation so that, after taking into account the various additional pulse broadening effects described below, detected pulse widths of the model pulsars are in reasonable agreement with the observations (see Fig. 4). Although the exact values of the above numerical factors are not crucial to our final results, models without this correlation built in were found to produce very unsatisfactory comparisons with the real sample.

Turning now to the instrumental terms in equation (4), we can insert the parameters of both surveys and write the dispersive

broadening across individual 3-MHz frequency channels as follows:

$$W_{\text{DM}} = 9.6 \mu\text{s} \left(\frac{\text{DM}}{\text{cm}^{-3} \text{ pc}} \right). \quad (6)$$

As described by Manchester et al. (2001), the sampling time t_{samp} depends on DM_{trial} . A file containing a list of trial DMs and sampling times is available as part of the online version of this article, available at <http://www.blackwell-synergy.com> (Table S2).

Finally, in order to model interstellar scattering, we make use of the well-known correlation between DM and the scattering time-scale t_{scatt} (see e.g. Slee, Dulk & Otrupcek 1980). Scaling the best-fitting relationship from the recent study of Bhat et al. (2004) to 1400 MHz, we find

$$\mathcal{T} = 0.154\mathcal{D} + 1.07\mathcal{D}^2 - 7, \quad (7)$$

where \mathcal{T} and \mathcal{D} are, respectively, the base-10 logarithms of t_{scatt} (in ms) and DM (in $\text{cm}^{-3} \text{ pc}$). To account for the dispersion about this relationship (see fig. 4 of Bhat et al. 2004), we dither the model scattering times using a normal distribution around \mathcal{T} with a standard deviation of 0.8.

The above discussion has detailed all the main steps in the simulation which allow us to calculate a predicted S/N for each model pulsar using equation (1). Those pulsars with S/Ns greater than 9 were deemed to be theoretically detectable. Each simulation proceeded until 25 000 model detectable pulsars were accumulated. This number was chosen to be much larger than the true sample size to minimize statistical fluctuations (see e.g. Bhattacharya et al. 1992). For each simulation, histograms of the observed distributions of P , \hat{L} , \hat{R} and \hat{z} were formed and normalized to have the same area as the sample of real observed pulsars.

To assess the overall quality of a simulation, we calculated the reduced- χ^2 statistic summed over the bins of the P , \hat{L} , \hat{R} and \hat{z} distributions. We note however that χ^2 is used here only as a figure of merit, and not as a means for hypothesis testing or rejection. For a typical starting model with flat PDFs in R , L , z and P the reduced χ^2 was, as expected, rather large, with typical values of the order of 1000. To improve these models, for each distribution, we computed a set of correction factors with one factor per bin defined as

$$C_i = \frac{R_i - M_i}{M_i}, \quad (8)$$

where R_i and M_i are, respectively, the real and model observed number of pulsars in the i th bin of one of the P , \hat{L} , \hat{R} and \hat{z} histograms. A new set of input distributions was then generated by multiplying each bin by the correction factor and adding this product to the original bin value. For example, the new z distribution, z' , is computed as follows:

$$z'_i = z_i + z_i \times C_i. \quad (9)$$

The resulting new set of PDFs should provide a better match to the observations. The simulation is then re-run and a new set of correction factors computed. We found that this procedure rapidly converged to produce a model with a much lower reduced χ^2 (typically of order unity) that stabilized after only a few iterations. We note in passing here that there appears to be very little covariance between the four PDFs. We found, through experimentation, that it was not possible to reach any satisfactory convergence by keeping one or more parameters constant during the iterations and varying the others. In this regard, at least within the overall limitations of the method we are using, we are confident that the models presented below are optimal and do not represent ‘local minima’ solutions.

4.3 A self-consistency test of the model

To verify that the above procedure can successfully recover the various Galactic distribution properties, we simulated two fake populations with different radial density functions. In the first population, pulsars were drawn from a simple Gaussian profile (see e.g. Narayan 1987) with a standard deviation of 6.5 kpc. For the second population, we adopted the more recent profile derived by Yusifov & Küçük (2004) which peaks at ~ 4 kpc and has a deficit of pulsars in the inner Galaxy. In both simulations, we assumed an exponential z distribution with a scaleheight of 350 pc (Mdžinarishvili & Melikidze 2004), a lognormal distribution of luminosities with a mean of -1.1 and standard deviation 0.9 (both in $\log 10$ of mJy kpc^2 , Faucher-Giguère & Kaspi 2006) and a gamma function for the spin periods which peaks at ~ 600 ms as described by Gil & Han (1996). The assumed pulse width versus period relationship was given in the previous section. Both models were run such that 1005 model pulsars were detected by our models of the PMB and PH surveys. The resulting model observed samples were then used as fake observed populations, i.e. for the purposes of this test, they take the place of the real observed sample.

After applying the Monte Carlo procedure described in the previous section to these fake samples, we were able to reproduce the functional form and correct number density over the parameter space of each model. Fig. 5 shows the results in terms of the input and derived radial density functions. These tests give us confidence that, when applied to the real observed sample of pulsars, our procedure provides a reliable means of estimating the true spatial and luminosity functions of pulsars in the Galaxy.

4.4 Application to the observed pulsar sample

We now apply the above procedure to the real sample of 1008 isolated pulsars detected by the PMB and PH surveys. As discussed above we consider two different cases: a ‘smooth’ (S) model of the Galaxy using the Lyne et al. (1985) electron density distribution and a ‘clumpy’ (C) model using the Cordes & Lazio (2002) electron density distribution and following the spiral-arm modelling described by Faucher-Giguère & Kaspi (2006). In each case, we computed distances to both the real and model pulsars using the appropriate electron density model.

Figs 6 and 7 show the real observed and resulting model underlying distribution functions derived from our analysis. The error bars shown here are purely statistical estimates with a fractional uncertainty equal to $1/\sqrt{N}$, where N is the number of observed pulsars in each bin. To parametrize our results in a form that may be of use to others, we also attempt to fit various analytic functions to the underlying distributions; these are shown by the smooth curves in each figure. For the radial density profile, we use a gamma function

$$\rho(R) = A \left(\frac{R}{R_{\odot}} \right)^B \exp \left[-C \left(\frac{R - R_{\odot}}{R_{\odot}} \right) \right]; \quad (10)$$

for the z distribution, we use the exponential function

$$N = D \exp \left(\frac{-|z|}{E} \right); \quad (11)$$

for the luminosity distribution, we fit a simple power law

$$\log N = F \log L + G; \quad (12)$$

finally, we fit the period distribution to the function

$$N(\log P) = H \exp \left[-\frac{(\log P - I)^2}{2J^2} \right]. \quad (13)$$

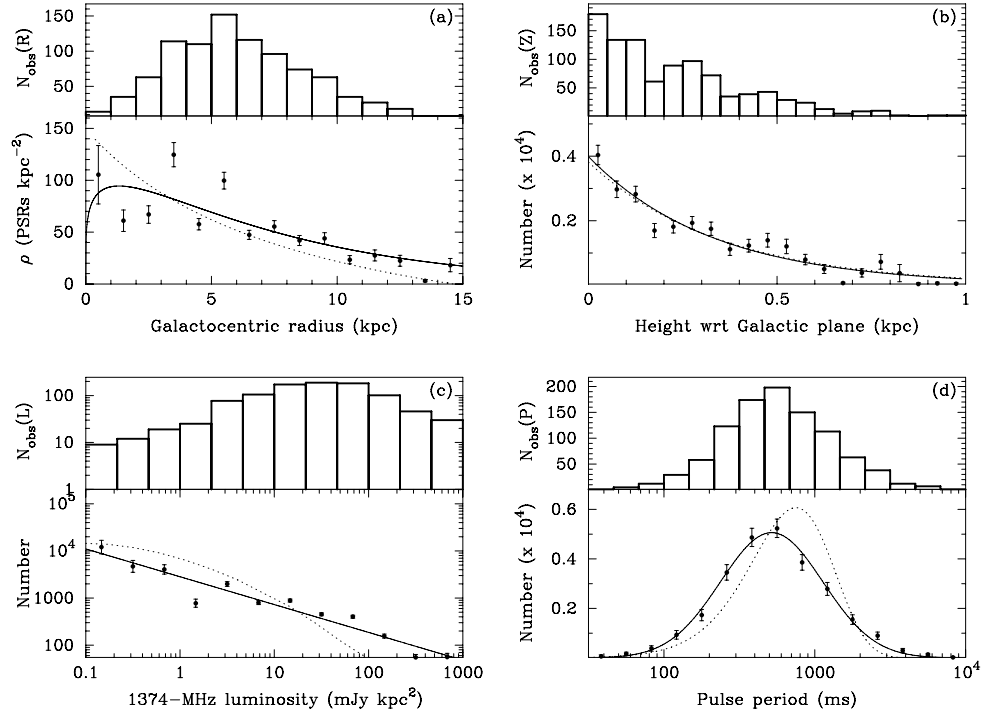


Figure 6. Observed number distribution from our input sample (upper panels) and derived distributions for model S (lower panels) for the parameters: (a) $\rho(R)$; (b) z ; (c) L and (d) P . The solid curves are the smooth analytic functions fitted to the data (see Section 4.4). The dotted curves show: (a) the assumed radial density function of free electrons used; (b) an exponential z distribution with a scaleheight of 350 pc; (c) a lognormal fit to the optimal pulsar population model derived by Faucher-Giguère & Kaspi (2006) and (d) a parent period distribution used by Kolonko et al. (2004) in a study of pulse-width statistics.

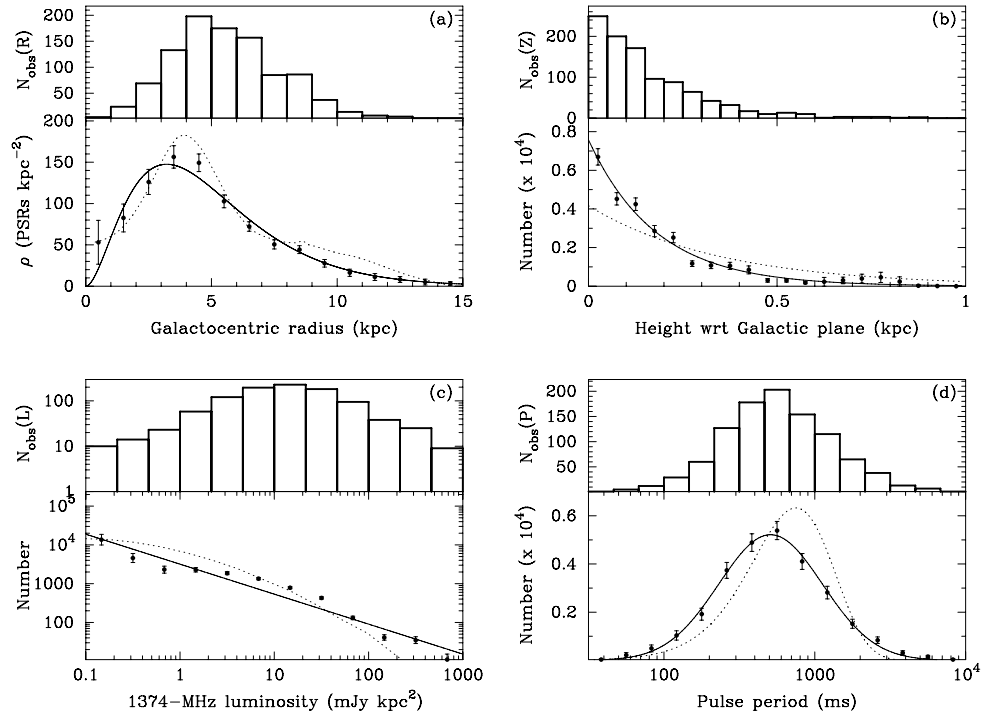


Figure 7. Observed number distribution from our input sample (top panels) and derived distributions for model C (lower panels) for the parameters: (a) $\rho(R)$; (b) z ; (c) L and (d) P . Solid and dotted curves are as described in the caption to Fig. 6.

Table 7. Summary of the analytic function fits to models S and C. The various parameters used are described in equations (10)–(13). Figures in parentheses give the 1σ uncertainty in the least significant digit.

Parameter	Model S fit	Model C fit	Unit
<i>A</i>	44(7)	41(5)	kpc^{-2}
<i>B</i>	0.2(2)	1.9(3)	
<i>C</i>	1.4(6)	5.0(6)	
<i>D</i>	0.39(2)	0.75(3)	
<i>E</i>	0.33(3)	0.18(1)	kpc
<i>F</i>	−0.59(5)	−0.77(7)	
<i>G</i>	3.45(8)	3.5(1)	
<i>H</i>	0.51(1)	0.52(1)	
<i>I</i>	2.71(1)	2.70(1)	
<i>J</i>	−0.34(1)	−0.34(1)	

Table 7 summarizes the resulting fit parameters *A* through *J* for both models. The dotted lines in the figures compare our results with various other distributions and are described in turn below.

4.5 Discussion of the results

4.5.1 Radial distribution

The underlying radial density distribution of each model provides a straightforward means of calculating the implied number of potentially detectable pulsars (i.e. above the luminosity threshold of 0.1 mJy kpc^2 and beaming towards us) in the Galaxy, N_G . For models S and C respectively we find $N_G = 28\,000 \pm 1100$ and $30\,000 \pm 1100$. Adopting the Tauris & Manchester (1998) beaming model, these numbers translate to $148\,000 \pm 6000$ and $155\,000 \pm 6000$ active radio pulsars in the Galaxy with luminosities above 0.1 mJy kpc^2 . While these numbers are consistent, the shape of the radial density distributions are quite different. As seen in Figs 6(a) and 7(a), where the dotted lines show the radial distribution of free electrons, we find that the pulsar distribution very closely follows that of the electrons in both cases. This striking correlation can be understood when one realizes that model C has an enhancement of electrons in the range $3 < R < 5 \text{ kpc}$. Thus, at low Galactic longitudes, the model will preferentially place pulsars either on the near side or on the far side of the Galaxy, close to the electron density enhancement. For model S, where the electron density peaks at $R = 0$, such pulsars are preferentially placed towards the centre of the Galaxy. These different radial distributions have implications for the detection rates of future surveys as we discuss later in Section 4.7.

We conclude from the above discussion that the Galactic pulsar and electron density distributions in the inner Galaxy are highly covariant. Based on our current state of knowledge, i.e. that the Cordes & Lazio (2002) model provides a far better description of the free electron distribution than all of its predecessors, our optimal model for the Galactic pulsar population is model C. However, given the uncertainty in the electron distribution in the inner Galaxy, care should be taken when interpreting the results of our fit which shows a peak in the pulsar distribution at 3–5 kpc. Further progress on the radial density distribution of pulsars requires independent distance estimates for more pulsars in the inner Galactic quadrants. Another possibility worth exploring, though beyond the scope of this paper, is to treat the electron density distribution as a free parameter in the Monte Carlo simulations. For now, we simply caution that the deficit of pulsars in the inner Galaxy noted here (see also the earlier

papers by Johnston 1994; Yusifov & Küçük 2004; Lorimer 2004) depends on the assumption of a corresponding deficit in the free electron density.

4.5.2 z distribution

We now consider an interesting result from our fits to the z distributions of both models, where it is seen that model S results in a scaleheight of 330 pc compared to only 180 pc for model C. The latter value is much lower than the canonical value of 300–350 pc expected a priori from an independent study of the local pulsar population (Mdžinarishvili & Melikidze 2004) and shown by the dotted line in Figs 6(b) and 7(b). As for the radial distribution, we believe this difference to be a direct result of the different electron density distributions used in the two models. From a comparison of Figs 6(b) and 7(b), we see that the z heights of the observed pulsar sample computed using the Lyne et al. (1985) electron density model are much broader than when using the Cordes & Lazio (2002) model.

The discrepancy is further highlighted when one utilizes the two other surveys carried out with the Parkes multibeam system, i.e. the Swinburne intermediate and high latitude pulsar surveys (respectively, SIL and SHL surveys, Edwards et al. 2001; Jacoby 2005). Along with the PH survey, these Swinburne surveys sample the distribution away from the Galactic plane and are therefore very sensitive to the z scaleheight of the pulsar population. As mentioned previously, these surveys were not included in the main analysis because the majority of pulsars from them do not have measured flux densities. However, our models should be able to reproduce the relative yield of the PMB and PH surveys alongside the SIL and SHL surveys. We have carried out such an analysis and compare the observed pulsar samples from these surveys with the various models in Table 9. As can be seen, the expected survey detections for model S are generally in good agreement with the actual survey results. For model C, however, the predicted yield for all surveys away from the Galactic plane is much lower than observed.

As a final sanity check, we have verified through additional simulations similar to those described in Section 4.3, that our modelling procedure is capable of reproducing any reasonable input scaleheight distribution. Based on these results, we conclude that there is a potential inconsistency when using the Cordes & Lazio (2002) model to derive the scaleheight of pulsars and consider a more likely value to be that found by model S, i.e. 330 pc. The apparent clustering of the PMB pulsars towards small z heights when using the Cordes & Lazio (2002) model was also noted by Kramer et al. (2003). It appears that further investigation of the z distribution in the electron density model is now warranted. While Mdžinarishvili & Melikidze (2004) also used the Cordes & Lazio (2002) electron density model, their analysis only considered pulsars within a cylinder of radius 3 kpc centred on the Sun. This local population analysis was done to minimize selection effects. Although our analysis attempts to correct for these effects as far as possible, we believe the Cordes & Lazio (2002) distance model is biasing our results towards an artificially lower scaleheight.

In an attempt to correct for this bias, we have introduced a modified version of model C, denoted by model C' , which is identical with the original model with the exception of having an exponential z distribution with a scaleheight of 330 pc. As can be seen from the yields of this model in Table 9, the revised scale height is in much better agreement with pulsar surveys carried out at higher Galactic latitudes. We return to this model for the discussions on pulsar current analysis and survey predictions (Sections 4.6 and 4.7).

4.5.3 Luminosity distribution

For both models S and C, we find that the simple power law given in equation (12) provides an adequate description of the underlying luminosity function for $L > 0.1$ mJy kpc². However, the slope of the distribution (-0.6 for model S and -0.8 for model C) is somewhat flatter than the canonical value $d \log N / d \log L = -1$ derived in early studies of the pulsar population (see e.g. Taylor & Manchester 1977). Overlaid on both Figs 6(c) and 7(c) is the lognormal fit to the luminosity distribution from the optimal model of Faucher-Giguère & Kaspi (2006). As can be seen, given the uncertainties involved, both models S and C are in reasonable agreement with the results of Faucher-Giguère & Kaspi (2006).

The behaviour of the luminosity function below 0.1 mJy kpc² is not well constrained by our analysis. Although we began our study using a luminosity distribution which extended to 0.01 mJy kpc², we found that the few pulsars in the observed sample with $L < 0.1$ mJy kpc² could be accounted for simply by a luminosity function with a lower limit of 0.1 mJy kpc² and the dithering of luminosities resulting from a 20 per cent distance uncertainty. Better constraints on the shape of the low end of the pulsar luminosity function should be possible from an analysis of deep targeted searches for young pulsars (for a recent review, see Camilo 2004).

4.5.4 Period distribution

In Figs 6(d) and 7(d), we compare our period distribution with the parent distribution favoured by Kolonko, Gil & Maciesiak (2004) in their analysis of pulse-width statistics. As can be seen, our distribution is significantly different, with a much higher proportion of short-period pulsars. Given the effort to quantify and account for period-dependent selection effects in this paper, we believe our fit using the lognormal distribution given in equation (13) provides a much better description of the parent population of normal pulsars and recommend its adoption in future pulse-width analyses.

4.6 Pulsar current analysis

To compute the birth rate of the population, we follow previous authors (Phinney & Blandford 1981; Vivekanand & Narayan 1981; Lorimer et al. 1993; Lyne et al. 1998; Vranesevic et al. 2004) and perform a pulsar current analysis. We closely follow the approach described in detail by Vranesevic et al. (2004) and calculate a weight or ‘scalefactor’ for each of the 1008 pulsars in our main sample. The analysis proceeds by placing each of these pulsars in every position of our model galaxy and recording the number of detections made by our model PMB and PH surveys. The model galaxy used for these calculations was model C’, i.e. the modified version of model C which has a z scaleheight of 330 pc and produces the best match to the other survey detection rates (see Section 4.5.2). To compute the apparent flux density, we use the observed luminosity of each pulsar and apply the empirical relationship given in equation (5) to calculate an intrinsic pulse width at each position in the model Galaxy. The scalefactor is then the ratio of the total number of positions tried to the number of detections found.

Having obtained a set of scalefactors, the current or flow of pulsars from short to longer periods can be calculated by binning the sample into period intervals of width ΔP . For a given period bin containing n_{psr} pulsars, following Vivekanand & Narayan (1981), we define the

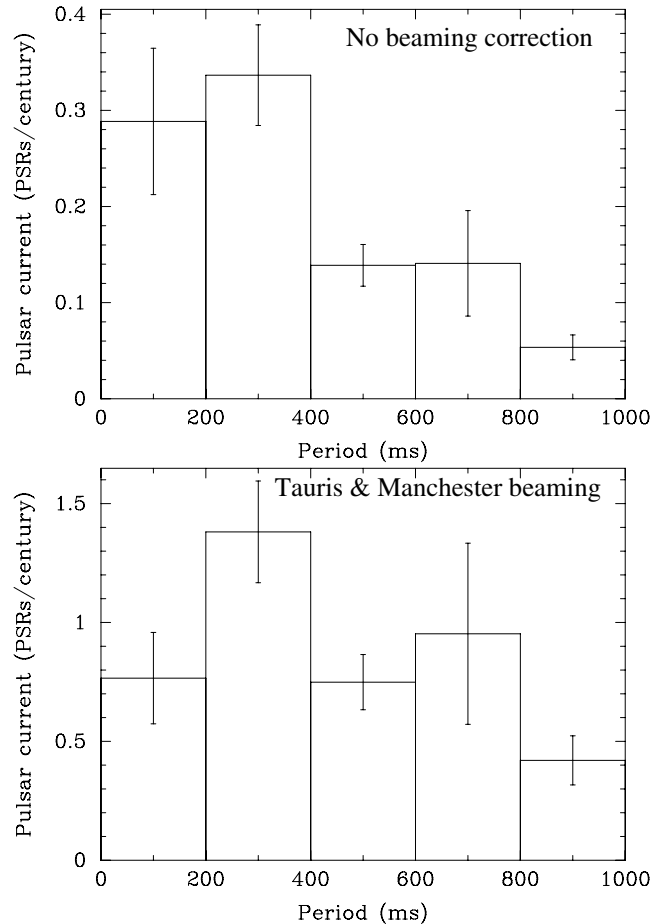


Figure 8. Histograms of pulsar current as a function of period showing the distribution for potentially observable pulsars (top panel) and after applying the beaming model of Tauris & Manchester (1998, bottom panel) with luminosities greater than 0.1 mJy kpc². The error bars shown are statistical estimates based on the sum of the squares of the individual scalefactors in each bin (Vivekanand & Narayan 1981).

pulsar current

$$J(P) = \frac{1}{\Delta P} \left(\sum_{i=1}^{n_{\text{psr}}} \frac{\xi_i \dot{P}_i}{f_i} \right), \quad (14)$$

where ξ_i is the scalefactor of the i th pulsar, with period derivative \dot{P}_i and f_i is the fraction of 4π sr of the sky covered by the radio beam. In the discussion below, we quote results for ‘potentially observable pulsars’ (i.e. $f_i = 1$) and assuming various beaming models for which $f_i < 1$. The uncertainty in the current for each period bin is dominated by the statistical error in the scalefactors. These are calculated, again following Vivekanand & Narayan (1981), as the square root of the sum of the squares of the scalefactors in each period bin.

A histogram of pulsar current versus period is shown for the population as a whole in Fig. 8 from which we infer a birth rate (i.e. maximum current value) of potentially observable pulsars with $L > 0.1$ mJy kpc² to be 0.34 ± 0.05 pulsars per century. As in earlier analysis, we find here no requirement for the birth (or ‘injection’) of pulsars with periods ~ 0.5 s. Following these authors, we have also examined the birth rate contribution as a function of inferred dipole magnetic field strength, B . Using the same grouping criteria as Vranesevic et al. (2004), we find birth rates of $0.04 \pm$

Table 8. A comparison of the birth rates derived from the pulsar current analysis as a function of luminosity cut-off and beaming model. Figures in parentheses represent statistical 1σ uncertainties in the least significant digit(s) calculated as the square root of the sum of the squares of the scale-factors in the maximum pulsar current bin (Vivekanand & Narayan 1981).

Beaming model	Minimum luminosity (mJy kpc ²)		
	0.1	1	10
No correction (i.e. $f = 1$)	0.34(5)	0.28(4)	0.12(3)
Tauris & Manchester (1998)	1.38(21)	1.14(18)	0.42(3)
Biggs (1990)	1.14(18)	0.94(15)	0.35(8)
Lyne & Manchester (1988)	1.32(21)	1.09(17)	0.41(9)
Narayan & Vivekanand (1983)	0.51(8)	0.43(7)	0.16(4)

0.02, 0.14 ± 0.07 and 0.16 ± 0.04 pulsars per century, respectively, for the low ($B < 9 \times 10^{11}$ G), medium ($9 \times 10^{11} \leq B \leq 2.5 \times 10^{12}$ G) and high ($B > 2.5 \times 10^{12}$ G) field populations. These results agree with the findings of Vranesevic et al. (2004).

In Table 8, we use various beaming models to apply a period-dependent correction to the pulsar current which accounts for those pulsars whose radiation beams do not intersect with our line of sight. We also break down these results for three different luminosity cut-offs: 0.1, 1 and 10 mJy kpc². For the three most recently published beaming models considered (Lyne & Manchester 1988; Biggs 1990; Tauris & Manchester 1998), the results are consistent within the uncertainties derived from the scalefactor statistics. For the earlier Narayan & Vivekanand (1983) model, in which the radio beams are elongated in the meridional direction, the birth rates are systematically lower. Regardless of the beaming model adopted, this compilation suggests that the majority (~ 80 per cent) of all pulsars appear to be born with luminosities $L > 1$ mJy kpc². It should be stressed, however, that the pulsar sample from which these results were obtained do not include the recent discoveries made in deep targeted searches of supernova remnants and X-ray point sources (Camilo 2004, and references therein). As was the case for the luminosity function discussed in Section 4.5.3, further insights into the birth luminosities of pulsars will await a statistical analysis of these discoveries from the targeted searches.

4.7 Predictions for other pulsar surveys

We have shown in Section 4.5.2 that our models have generally provided a good match to the yields of existing pulsar surveys. It is therefore natural to apply these models to make some predictions of the number of pulsars expected in ongoing surveys. In Table 9, we list the number of expected pulsar detections for two such projects: the Perseus Arm (PA) survey being carried out at Parkes and PALFA, a pulsar survey with the seven-beam Arecibo *L*-band Feed Array (ALFA) system (Cordes et al. 2006; Lorimer et al. 2006). Note that the predictions below refer to normal pulsars only.

The PA survey is extending the Galactic plane coverage of the PMB survey to the region $-160^\circ < l < -100^\circ$ and $|b| < 5^\circ$ where there are currently 17 non-recycled pulsars. With the exception of a data sampling interval of 125 μ s, the PA survey uses identical observing parameters and data acquisition and processing schemes to those implemented in PMB survey. Since the PA survey is targeting pulsars outside the solar circle, the expected yield is strongly dependent on the radial distribution in the outer Galaxy. This can be seen by comparing the number of detections for model S (62) and C' (32). Upon completion, it is expected that this survey will

Table 9. A comparison of the number of detected pulsars for the real sample with several models developed in this paper for the various pulsar surveys. The completed pulsar surveys are the Parkes multibeam survey (this paper, PMB), the Swinburne intermediate latitude survey (Edwards et al. 2001, SIL), the Parkes high-latitude survey (Burgay et al. 2006, PH), the Swinburne high-latitude survey (Jacoby 2005, SHL). Pulsar surveys which are currently ongoing are the Perseus arm (PA) survey with the Parkes multibeam system and the PALFA surveys with Arecibo (Cordes et al. 2006). PALFAi refers to the inner Galaxy survey, while PALFAa refers to the anticentre survey. For the completed pulsar surveys, the column labeled ‘Real’ lists the number of pulsars detected (i.e. discoveries and redetections). For the ongoing surveys the numbers marked with a * refer to currently known pulsars in the survey regions with flux densities higher than the nominal survey threshold. The remaining columns are the average number of predicted detections using each model.

Survey	Real	Model S	Model C	Model C'
Completed pulsar surveys				
PMB	986	967	991	984
SIL	156	146	88	160
PH	32	33	23	30
SHL	51	52	17	38
Ongoing pulsar surveys				
PA	17*	62	35	32
PALFAi	200*	480	550	530
PALFAa	6*	54	30	30

provide excellent constraints on the radial distribution for $R > 8.5$ kpc.

The PALFA survey is currently observing two regions of the Galactic plane visible from Arecibo with $|b| < 5^\circ$ at an observing frequency of 1.4 GHz. The inner Galaxy survey (PALFAi) covers the region $32^\circ < l < 77^\circ$ while the anticentre survey (PALFAa) covers the region $168^\circ < l < 214^\circ$. A detailed description of the survey parameters and initial discoveries can be found in Cordes et al. (2006). Prior to these surveys, the number of normal pulsars known in these ranges was 200 for the inner Galaxy and six for the anticentre. Models S and C therefore predict of the order of 350 new discoveries in the inner Galaxy. While this is significantly lower than estimates made by Cordes et al. (2006), it is consistent with recent independent work carried out by Faucher-Giguère & Kaspi (private communication). As for the PA survey, the lower expected PALFA yields in the anticentre region (of the order of 50 or 25 discoveries for models S and C) depend sensitively on the radial density function in the outer Galaxy.

5 CONCLUSIONS

We have presented discovery and follow-up parameters for 142 pulsars discovered in the Parkes multibeam survey. Using a sample of 1008 normal pulsars from this survey and the Parkes high-latitude survey, we have carried out Monte Carlo simulations to investigate various aspects of the Galactic population. Our main conclusions are as follows.

- (i) The derived Galactic distribution of pulsars and assumed distribution of free electrons in the Galaxy are strongly coupled. Based on the electron density model of Cordes & Lazio (2002), we infer a radial distribution for the pulsar population which peaks at 4 kpc from the Galactic Centre. Although further surveys at higher frequencies will be useful, it is more important to have independent

constraints on the distances to currently known pulsars in this region to confirm the proposed radial distribution.

(ii) The z distribution as inferred from our simulations is also strongly influenced by the electron density model used. Using the Cordes & Lazio (2002) model in our simulations, the best-fitting model population underpredicts the number of pulsars found in the Swinburne intermediate- and high-latitude surveys. To overcome this bias, we have increased the scaleheight of the model population to 330 pc. We believe that this apparent inconsistency will provide a very useful constraint for future revisions of the Galactic distribution of free electrons.

(iii) The luminosity distribution we derive follows a simple power law with a slope of $d \log N / d \log L \sim -0.8$. While this is somewhat flatter than previous estimates, our luminosity function is consistent with that derived independently by Faucher-Giguère & Kaspi (2006). The shape of the luminosity function below 0.1 mJy kpc² is not well constrained by our analysis. Although six pulsars with $L < 0.1$ mJy kpc² are known in our current sample, their existence can be explained by distance uncertainties and a luminosity function with a lower bound at 0.1 mJy kpc². We stress again here that an analysis of recent discoveries of faint young pulsars in targeted searches will provide further constraints on the luminosity function of pulsars below 0.1 mJy kpc².

(iv) Applying a pulsar current analysis to the observed sample and a modified version of model C, we find the birth rate of the potentially observable population to be 0.34 ± 0.05 pulsars per century. Applying the Tauris & Manchester (1998) beaming model to account for unbeamed pulsars, we find a birth rate of 1.4 ± 0.2 pulsars per century for luminosities above 0.1 mJy kpc². There is no evidence for any injection of pulsars with birth periods ~ 0.5 s into the population. We agree with the findings of Vranesevic et al. (2004) that most of the birth rate comes from high magnetic field pulsars.

(v) Predictions for current surveys of the outer Galaxy at Parkes and Arecibo depend sensitively on the form of the radial distribution outside the solar circle. Although this distribution is poorly known at present these surveys are expected to provide further constraints in the near future. The Arecibo multibeam survey of the inner Galaxy is expected to yield of the order of 350 new discoveries. We expect these surveys to provide further constraints on the population parameters derived in this work.

The Parkes multibeam surveys provide a superb data base with which to study various aspects of the pulsar population. The analysis presented here has attempted to be as straightforward as possible with the minimum of assumptions made. Further more detailed studies such as presented recently by Faucher-Giguère & Kaspi (2006) are warranted and will certainly provide further insights into the underlying population properties discussed here.

ACKNOWLEDGMENTS

We thank Simon Johnston for useful discussions concerning the radial density distribution of pulsars and Claude-Andr e Faucher-Gigu ere for comments on an earlier version of this manuscript. We gratefully acknowledge technical assistance with hardware and software provided by Jodrell Bank Observatory, CSIRO ATNF, Osservatorio Astronomico di Cagliari and the Swinburne centre for Astrophysics and Supercomputing. The Parkes radio telescope is part of the Australia Telescope which is funded by the Commonwealth of Australia for operation as a National Facility managed by CSIRO. The Arecibo Observatory, a facility of the National Astronomy and

Ionosphere Centre, is operated by Cornell University under a cooperative agreement with the US National Science Foundation. DRL was a University Research Fellow funded by the Royal Society for the duration of most of this work. IHS holds an NSERC UFA and is supported by a Discovery Grant. FC acknowledges support from NSF grant AST-05-07376. NDA, AP and MB received support from the Italian Ministry of University and Research under the national program PRIN-MIUR 2005. This work made use of the facilities of the ATNF Pulsar Catalogue.

REFERENCES

- Arzoumanian Z., Chernoff D. F., Cordes J. M., 2002, *ApJ*, 568, 289
 Bailes M. et al., 1997, *ApJ*, 481, 386
 Baring M. G., Harding A. K., 2001, *ApJ*, 547, 929
 Bhat N. D. R., Cordes J. M., Camilo F., Nice D. J., Lorimer D. R., 2004, *ApJ*, 605, 759
 Bhattacharya D., van den Heuvel E. P. J., 1991, *Phys. Rep.*, 203, 1
 Bhattacharya D., Wijers R. A. M. J., Hartman J. W., Verbunt F., 1992, *A&A*, 254, 198
 Biggs J. D., 1990, *MNRAS*, 245, 514
 Blandford R. D., Teukolsky S. A., 1976, *ApJ*, 202, 580
 Brogan C. L., Gelfand J. D., Gaensler B. M., Kassim N. E., Lazio T. J. W., 2006, *ApJ*, 639, L25
 Burgay M. et al., 2006, *MNRAS*, 368, 283
 Camilo F., 2004, in Camilo F., Gaensler B. M., eds, *IAU Symp. 218, Young Neutron Stars and Their Environments*. Astron. Soc. Pac., San Francisco, p. 97
 Camilo F., Nice D. J., Taylor J. H., 1993, *ApJ*, 412, L37
 Camilo F., Nice D. J., Shrauner J. A., Taylor J. H., 1996, *ApJ*, 469, 819
 Camilo F. et al., 2004, *ApJ*, 611, L25
 Cordes J. M. et al., 2006, *ApJ*, 637, 446
 Cordes J. M., Lazio T. J. W., 2002, preprint (astro-ph/0207156)
 Dewey R., Stokes G., Segelstein D., Taylor J., Weisberg J., 1984, in Reynolds S., Stinebring D., eds, *Millisecond Pulsars*. NRAO, Green Bank, p. 234
 Edwards R. T., Bailes M., 2001, *ApJ*, 547, L37
 Edwards R. T., Bailes M., van Straten W., Britton M. C., 2001, *MNRAS*, 326, 358
 Faucher-Gigu ere C.-A., Kaspi V. M., 2006, *ApJ*, 643, 332
 Faulkner A. J. et al., 2004, *MNRAS*, 355, 147
 Faulkner A. J. et al., 2005, *ApJ*, 618, L119
 Gaensler B. M., Johnston S., 1995, *PASA*, 12, 76
 Gil J. A., Han J. L., 1996, *ApJ*, 458, 265
 G omez G. C., Benjamin R. A., Cox D. P., 2001, *AJ*, 122, 908
 Haslam C. G. T., Stoffel H., Salter C. J., Wilson W. E., 1982, *A&AS*, 47, 1
 Hobbs G. et al., 2004, *MNRAS*, 352, 1439
 Hotan A. W., van Straten W., Manchester R. N., 2004, *PASA*, 21, 302
 Jacoby B. A., 2005, PhD thesis, CalTech
 Johnston S., 1994, *MNRAS*, 268, 595
 Kolonko M., Gil J., Maciesiak K., 2004, *A&A*, 428, 943
 Kramer M., Xilouris K. M., Lorimer D. R., Doroshenko O., Jessner A., Wielebinski R., Wolszczan A., Camilo F., 1998, *ApJ*, 501, 270
 Kramer M. et al., 2003, *MNRAS*, 342, 1299
 Lange C., Camilo F., Wex N., Kramer M., Backer D., Lyne A., Doroshenko O., 2001, *MNRAS*, 326, 274
 Large M. I., 1971, in Davies R. D., Smith F. G., eds, *IAU Symp. 46, The Comparative Properties of the Pulsars*. Reidel, Dordrecht, p. 165
 Lawson K. D., Mayer C. J., Osborne J. L., Parkinson M. L., 1987, *MNRAS*, 225, 307
 Lommen A. N., Kipporn R. A., Nice D. J., Splaver E. M., Stairs I. H., Backer D. C., 2006, *ApJ*, 642, 1012
 Lorimer D. R., 2004, in Camilo F., Gaensler B. M., eds, *IAU Symp. 218, Young Neutron Stars and Their Environments*. Astron. Soc. Pac., San Francisco, p. 105
 Lorimer D. R., Bailes M., Dewey R. J., Harrison P. A., 1993, *MNRAS*, 263, 403

- Lorimer D. R., Kramer M., 2005, *Handbook of Pulsar Astronomy*. Cambridge Univ. Press, Cambridge
- Lorimer D. R., Lyne A. G., Camilo F., 1998, *A&A*, 331, 1002
- Lorimer D. R. et al., 2004, *MNRAS*, 347, L21
- Lorimer D. R. et al., 2006, *ApJ*, 640, 428
- Lyne A. G., Manchester R. N., 1988, *MNRAS*, 234, 477
- Lyne A. G. et al., 1998, *MNRAS*, 295, 743
- Lyne A. G., Manchester R. N., Taylor J. H., 1985, *MNRAS*, 213, 613
- McLaughlin M. A. et al., 2006, *Nat*, 439, 817
- Manchester R. N. et al., 2001, *MNRAS*, 328, 17
- Mdzinarishvili T. G., Melikidze G. I., 2004, *A&A*, 425, 1009
- Morris D. J. et al., 2002, *MNRAS*, 335, 275
- Narayan R., 1987, *ApJ*, 319, 162
- Narayan R., Popham R., 1989, *ApJ*, 346, L25
- Narayan R., Vivekanand M., 1983, *A&A*, 122, 45
- Phinney E. S., 1992, *Philos. Trans. Roy. Soc. London A*, 341, 39
- Phinney E. S., Blandford R. D., 1981, *MNRAS*, 194, 137
- Ruderman M. A., Sutherland P. G., 1975, *ApJ*, 196, 51
- Slee O. B., Dulk G. A., Otrupcek R. E., 1980, *PASA*, 4, 100
- Stairs I. H. et al., 2005, *ApJ*, 632, 1060
- Tauris T. M., Manchester R. N., 1998, *MNRAS*, 298, 625
- Taylor J. H., Cordes J. M., 1993, *ApJ*, 411, 674
- Taylor J. H., Manchester R. N., 1977, *ApJ*, 215, 885
- van den Heuvel E. P. J., Bitzaraki O., 1995, in Alpar A., Kiziloğlu Ü., van Paradis J., eds, *The Lives of the Neutron Stars (NATO ASI Series) X-ray Binaries and Recycled Pulsars*. Kluwer, Dordrecht, p. 421
- Vivekanand M., Narayan R., 1981, *J. Astrophys. Astr.*, 2, 315
- Vranesevic N. et al., 2004, *ApJ*, 617, L139
- Young M. D., Manchester R. N., Johnston S., 1999, *Nat*, 400, 848
- Yusifov I., Küçük I., 2004, *A&A*, 422, 545

SUPPLEMENTARY MATERIAL

The following supplementary material is available for this article online:

Table S1. File showing Galactic coordinates and beam number for the multibeam survey.

Table S2. List of trail dispersion measure and sampling times used in the PMB survey.

This material is available as part of the online article from <http://www.blackwell-synergy.com>

This paper has been typeset from a \TeX/L\TeX file prepared by the author.